

# 1 Trial-by-trial inter-areal interactions 2 in visual cortex in the presence or 3 absence of visual stimulation

4 **Dianna Hidalgo**<sup>1\*†</sup>, **Giorgia Dellaferrera**<sup>2†</sup>, **Will Xiao**<sup>1</sup>, **Maria Papadopoulou**<sup>3,4</sup>, **Stelios**  
5 **Smirnakis**<sup>1,5</sup>, **Gabriel Kreiman**<sup>2\*</sup>

**\*For correspondence:**

[gabriel.kreiman@tch.harvard.edu](mailto:gabriel.kreiman@tch.harvard.edu)  
(GK); [diannahidalgo@g.harvard.edu](mailto:diannahidalgo@g.harvard.edu)  
(DH)

†These authors contributed  
equally to this work

6 <sup>1</sup>Department of Neurobiology, Harvard Medical School, Boston, MA, USA.; <sup>2</sup>Children's  
7 Hospital, Harvard Medical School, Boston, MA, USA.; <sup>3</sup>Department of Computer Science,  
8 University of Crete, Heraklion, Greece; <sup>4</sup>Institute of Computer Science, FORTH,  
9 Heraklion, Greece; <sup>5</sup>Department of Neurology, Brigham and Women's Hospital,  
10 Boston, MA, USA

---

12 **Abstract** State-of-the-art computational models of vision largely focus on fitting trial-averaged  
13 spike counts to visual stimuli using overparameterized neural networks. However, a  
14 computational model of the visual cortex should predict the dynamic responses of neurons in  
15 single trials across different experimental conditions. In this study, we investigated trial-by-trial  
16 inter-areal interactions in the visual cortex by predicting neuronal activity in one area based on  
17 activity in another, distinguishing between stimulus-driven and non-stimulus-driven shared  
18 variability. We analyzed two datasets: calcium imaging from mouse V1 layers 2/3 and 4, and  
19 extracellular neurophysiological recordings from macaque V1 and V4. Our results show that  
20 neuronal activity can be predicted bidirectionally between L2/3 and L4 in mice, and between V1  
21 and V4 in macaques, with the latter interaction exhibiting directional asymmetry. The  
22 predictability of neuronal responses varied with the type of visual stimulus, yet responses could  
23 also be predicted in the absence of visual stimulation. In mice, we observed a bimodal  
24 distribution of neurons, with some neurons primarily driven by visual inputs and others showing  
25 predictable activity during spontaneous activity despite lacking consistent visually evoked  
26 responses. Predictability also depended on intrinsic neuronal properties, receptive field overlap,  
27 and the relative timing of activity across areas. Our findings highlight the presence of both  
28 stimulus- and non-stimulus-related components in interactions between visual areas across  
29 diverse contexts and underscore the importance of non-visual shared variability between visual  
30 regions in both mice and macaques.

---

## 32 Introduction

33 To predict the activity of neurons in the visual cortex, multiple studies have focused on correlat-  
34 ing external stimuli with trial-averaged responses (*Hubel and Wiesel, 1962; Pasupathy et al., 2020*).  
35 Between the stimulus and cortical neurons, there is a complex signal processing cascade involving  
36 multiple processing stages. Therefore, computational models of visual processing typically gloss  
37 over most of the relevant biological machinery in an attempt to fit average firing rates from images  
38 (*Serre et al., 2007a; Yamins et al., 2014*). A mechanistic understanding of the factors that govern  
39 firing in the visual cortex requires models that can capture the trial-by-trial transformations across  
40 those processing stages. Moreover, neurons throughout the cortex fire “spontaneously” in the

41 absence of any visual input. Thus, by definition, any model predicting neuronal activity that is ex-  
42 clusively dependent on visual stimulation does not account for such fluctuations. Previous studies  
43 in mice have revealed significant non-visual influences in neuronal activity in cortex, even in V1,  
44 partly accounted for by movement (*Stringer et al., 2019b; Avitan and Stringer, 2022; Polack et al.,*  
45 *2013; Niell and Stryker, 2010; Dadarlat and Stryker, 2017*). These observations contrast with a re-  
46 cent macaque study which did not find the same motor-related spontaneous activity in either V1,  
47 V2, or V3 (*Talluri et al., 2023*). Nevertheless, variables that are not related to movement, such as  
48 attention, expectation, and arousal, also modulate stimulus- and non-stimulus driven neuronal ac-  
49 tivity in monkeys (*Reynolds and Chelazzi, 2004; Gazzaley et al., 2007; Okazaki et al., 2008; Gilbert*  
50 *and Li, 2013*), potentially adding to the response variability across stimulus repeats and to neuronal  
51 activity in the absence of visual stimuli.

52 Neuronal interactions between visual areas occur in the presence and absence of visual stimuli  
53 (*Chen et al., 2022; Stringer et al., 2019b; Wosniack et al., 2021; Ringach, 2009; Avitan and Stringer,*  
54 *2022*). Therefore, such interactions can and should be studied both as a function of sensory inputs  
55 and contextual cues but also in the absence of external stimulation or task demands (*Chacron*  
56 *et al., 2003; Hsu et al., 2004; Ringach, 2009*). A paradigmatic example of inter-area interactions  
57 is the series of synaptically-connected laminar (e.g. layer 4 → layer 2/3) and cortical areas (e.g.  
58 V1→V2→V4→IT) within the ventral visual stream (*Lee et al., 2016; Felleman and Van Essen, 1991;*  
59 *Markov et al., 2014; Douglas and Martin, 2004; Wang and Burkhalter, 2007; Consortium et al.,*  
60 *2021*). Due to feedforward, feedback, and horizontal connections in the ventral visual stream, the  
61 inter-areal interactions could represent shared visual and non-visual reliable information. Several  
62 studies examined *in vivo* interactions between visual areas in mice and macaques, focusing on  
63 the entire population level (*Semedo et al., 2019, 2022; Tang et al., 2023; Morales-Gregorio et al.,*  
64 *2024*), trial-averaged responses removing transient fluctuations (*Semedo et al., 2019*), neuronal  
65 activity in response to only one image presentation (*Semedo et al., 2019, 2022*), or in the absence  
66 of any stimulus (*Morales-Gregorio et al., 2024*). Here we investigated interactions between areas  
67 in single trials at the level of cortical layers or brain areas across different stimulus types or in the  
68 absence of visual stimulation, across different species, and across different recording techniques  
69 and temporal resolutions. We focused on multiple simultaneously recorded areas of the ventral  
70 visual stream to assess the stimulus- and non-stimulus-driven variability shared between cortical  
71 subnetworks. We found that it is possible to reciprocally predict neuronal activity, both during  
72 visual stimulation but also during spontaneous activity, and that this predictability depends on the  
73 intrinsic properties of each neuron, the degree of receptive field overlap, and the relative timing  
74 of activity across areas.

## 75 Results

### 76 Layer 4 activity predicts layer 2/3 activity and V1 activity predicts V4 activity in 77 single trials

78 We studied neuronal activity from two open datasets: mouse neurons in V1 layer 4 and layers 2/3  
79 (L4 and L2/3; calcium imaging; *Figure 1A*) (*Stringer et al., 2019a*), and macaque multiunit sites in  
80 areas V1 and V4 (extracellular electrophysiology; *Figure 1B*) (*Chen et al., 2022*). The mouse neu-  
81 ron recordings we used for this experiment were based on approx. 5,500 per mouse (n=4, *Table 1*)  
82 responding to visual stimuli (drifting gratings or static natural black and white images; to-  
83 tal of 7 recording days), in addition to “spontaneous” activity during approximately 30 minutes of  
84 gray/black screen presentation on 6 of the 7 recording days. The macaque recordings were based  
85 on 688 out of the 1,024 channels (n=1, *Table 2*) responding to visual stimuli (full-size static checker-  
86 board image, small and thin bar slow-moving in a small clockwise square direction; large and thick  
87 bar fast-moving in a big clockwise square direction; total of 5 recording days) in addition to spon-  
88 taneous activity during gray screen presentation in all recording days. There was also a lights-off  
89 condition, where the head-fixed monkey was free to open or close eyes for approximately 25 min-

90 utes in 3 our of the 5 recording days. We omitted some of the 1,024 channels with signal-to-noise  
91 ratio of less than 2, or that were considered “spurious” by the authors of the ope dataset (*Chen*  
92 *et al., 2022*).

93 We examined two types of interactions between areas: inter-laminar (*Figure 1C*; mouse V1)  
94 and inter-cortical (*Figure 1D*; macaque). We used linear ridge regression to predict neuronal ac-  
95 tivity in one area from activity in the other area in single trials (*Figure 1E*) (*Semedo et al., 2019*).  
96 Performance was evaluated using cross-validation over trials and quantified as squared Pearson’s  
97  $r$  (hereafter, “explained variance” or EV, *Methods*). *Figure 2A* shows sample neuronal activity from  
98 three example mouse V1 L2/3 cells during image presentation (black traces). Overlaid, the figure  
99 also shows the predicted neuronal activity (red). The predicted neuronal activity is shown as a  
100 function of the actual activity in response to every image presentation for the same example cells  
101 in *Figure 2C*. The top cell illustrates a case where the predicted activity closely matches the actual  
102 actual activity ( $EV = 0.67$ ), the middle cell shows a typical case ( $EV = 0.39$ ), and the bottom cell  
103 illustrates a case where the predictions deviated from the actual neuronal activity ( $EV = 0.07$ ). We  
104 focused on neurons deemed “visually responsive” (~17% of total L2/3 neurons; *Table 1*, *Methods*,  
105 see results for all neurons in *Figure Supplement 1*). The ridge regression model predicted single-  
106 trial L2/3 activity from L4 activity across both types of visual stimuli with an average EV of  $0.28 \pm$   
107  $0.16$  (mean  $\pm$  stdev. across neurons, *Figure 2E*) whereas the shuffle control mean EV was  $0.004 \pm$   
108  $0.002$  (see results for individual mice in *Figure Supplement 1*).

109 In the macaque, trial-to-trial variations in V4 activity were predicted from V1 activity across  
110 the three types of visual stimuli. Example recording sites are shown in *Figure 2B*, D. The ridge  
111 regression model predicted the single-trial responses in V4 activity from V1 activity with an average  
112 EV of  $0.34 \pm 0.15$  (*Figure 2F* whereas the shuffle control mean EV was  $0.005 \pm 0.005$ . There were  
113 few sites that were not visually responsive in macaques; EV results for all sites are shown in *Figure*  
114 *Supplement 1*).

115 In sum, it was possible to provide estimates of neuronal activity in single trials in both species,  
116 across different layers within primary visual cortex in mice and across different visual cortical areas  
117 in monkeys.

### 118 **Inter-cortical predictions are asymmetrical**

119 In the previous section, we demonstrated the possibility of predicting L2/3 activity from L4 activity  
120 and V4 from V1. We asked whether we could also predict neuronal responses in the opposite direc-  
121 tion. To directly compare predictability between directions in mouse and macaque, we matched  
122 the number of predictors (i.e., number of neurons/sites used to predict activity) and the degree of  
123 self-consistency (split-half  $r$  values) by randomly subsampling in each layer or cortical region prior  
124 to computing the predictability metrics (*Figure 3A*, C, *Methods*).

125 In mice, it was possible to predict L4 neuronal activity from the activity of populations of neurons  
126 in L2/3 and there was no statistically significant difference between the two directions ( $p > 0.05$ ,  
127 hierarchical permutation test, *Figure 3B*). When using the entire layer populations to predict each  
128 other’s neural activity (923-2,369 cells in L4, 5,420-7,980 cells in L2/3), L2/3 could predict L4 better  
129 than the reverse direction ( $p < 0.05$ , *Figure Supplement 2G*).

130 In macaques, while we could also predict V1 activity from the activity of a population of neurons  
131 in V4, when controlling for neuron number and split-half correlation values, the EV fraction in the  
132 V1→V4 direction was higher than in the V4→V1 direction ( $p < 0.001$ , *Figure 3D*). Even without con-  
133 trolling for the number of predictors or their respective split-half correlation values (627-688 sites  
134 in V1, 86-115 sites in V4), we found better predictability in the V1 to V4 direction than the reverse  
135 ( $p < 0.001$ , *Figure Supplement 2I*).

### 136 **Predictability of neuronal activity is dependent on the visual stimulus**

137 We evaluated whether the predictability of neuronal activity varied with the type of visual stimulus  
138 presented to the animal. In mice, we compared the inter-laminar prediction of neuronal activity of

139 visually responsive neurons in response to drifting gratings versus natural images (**Figure 4A**). We  
140 could predict mouse L4 and L2/3 activity under both stimulus conditions ( $p < 0.001$ , paired permuta-  
141 tion test of prediction vs. shuffled frames prediction). Predictability was higher for drifting gratings  
142 than natural images in the L4→L2/3 direction (**Figure 4B**;  $p < 0.001$ , hierarchical permutation test).

143 In macaques, we compared inter-cortical predictability of visually responsive site recordings in  
144 responses to a slow-moving small thin bar, fast-moving large thick bar, and a full-size checkerboard  
145 image (**Figure 4C**). We could predict V1 and V4 activity across all stimulus types ( $p < 0.001$ , paired  
146 permutation test of prediction vs. shuffled frames prediction). The predictability was the highest  
147 in both directions for neuronal activity in response to a full field checkerboard images (**Figure 4D**).  
148 In the V1→V4 direction, the EV fraction was higher when predicting a slow moving small thin bar  
149 compared to a fast moving large thick bar (**Figure 4D**, left), where as the opposite was true for the  
150 V4→V1 direction (**Figure 4D**, right).

### 151 **Neuronal activity could be predicted even during spontaneous activity**

152 Given the dependence on the visual stimulus, we next asked whether it would be possible to predict  
153 neuronal responses in the absence of any visual stimulus, during “spontaneous activity”. We com-  
154 pared the predictability of stimulus-evoked activity in mice (drifting gratings and natural images)  
155 versus the predictability of activity recorded during gray screen presentation. This comparison was  
156 conducted in both visually (SNR  $>2$  & split-half  $r >0.8$ ) and non-visually (SNR  $<2$  & split-half  $r <0.8$ )  
157 responsive neurons (n=3 mice; mouse MP027 did not undergo 30 min. of gray screen presenta-  
158 tion). In visually responsive neurons, there was a significant reduction in EV during gray screen  
159 compared to visual stimulus presentation (**Figure 5A** left,  $p < 0.001$ , hierarchical paired permuta-  
160 tion test). In contrast, for non-visually responsive neurons, predictability was higher during the  
161 gray screen condition (**Figure 5A** right,  $p < 0.001$ , hierarchical paired permutation test). Addition-  
162 ally, there was no correlation between neuronal predictability in the responses to visual stimulus  
163 presentations and in the response to gray screen presentations in visually responsive neurons  
164 (**Figure 5B**) but there was a strong correlation for non-visually responsive neurons (**Figure 5C**). The  
165 difference in predictability in the absence of a stimulus could in principle change according to the  
166 directionality in inter-laminar interactions. There was no statistically significant difference in the  
167 EV fraction between laminar directions (L4→L2/3 vs. L2/3→L4) using the same control population  
168 as in **Figure 3B** (**Figure 5A-C** and **Figure Supplement 2H**).

169 In macaques, we focused on visually responsive sites since the majority of the neuronal popu-  
170 lation was visually responsive (**Figure Supplement 1D**). Additionally, an SNR of less than 2 (one of  
171 the requirements to define non-visual neurons in the mouse data) most likely reflects artefactual  
172 issues with the electrode recording the multiunit site (**Chen et al., 2022**). We compared inter-areal  
173 prediction of stimulus presentation activity (checkerboard images and moving bars), gray screen  
174 presentation, and during lights-off. Similar to the conclusions drawn from the mouse data, the pre-  
175 dictability of neuronal activity was higher in response to stimulus presentation than to gray screen  
176 presentations (**Figure 5D** for checkerboard presentations, **Figure Supplement 4D** for moving bars;  
177  $p < 0.001$ , paired permutation test). However, the EV fraction in the lights-off condition was sig-  
178 nificantly higher than during the stimulus presentations in both directions. Eye closure and sleep  
179 can induce global oscillations (**Hohaia et al., 2022**) and therefore may correlate neuronal activity,  
180 causing an increase in predictability. To test this idea, we further separated the lights-off neu-  
181 ronral activity into periods where the macaque’s eyes were open or closed. The EV was higher than  
182 stimulus presentation activity only during the eyes-closed period (**Figure 5D**). Unlike the mouse,  
183 macaque correlation of visual predictability between stimulus presentation and spontaneous ac-  
184 tivity was high across all types of spontaneous conditions (**Figure 5E**, **Figure Supplement 4C**). When  
185 assessing the inter-cortical prediction directionality during spontaneous conditions, we found the  
186 same asymmetrical relationship as in **Figure 3**, where V1→V4 EV fraction was significantly higher  
187 than V4→V1 prediction in both gray screen ( $p < 0.01$ , permutation test) and lights-off ( $p < 0.001$ ,  
188 permutation test) conditions (**Figure Supplement 2G**).

## 189 **Receptive field overlap and neuronal response properties impact predictability**

190 We investigated which neuronal properties are related to the ability to predict responses by com-  
191 paring EV and key indicators of neuronal response reliability and receptive field properties, in both  
192 visually- and non-visually responsive neurons, during either visual presentations or spontaneous  
193 conditions. First, we considered the following properties: (i) max  $r^2$  value (i.e., maximum squared  
194 correlation between each neuron in the predictor population and the predicted neuron), (ii) 1-vs-  
195 rest  $r^2$  (the squared correlation of one neuron's activity across all stimuli with the mean neuron  
196 activity of the rest of the population), (iii) SNR of the predicted neuron, (iv) variance across stim-  
197 uli (computed for mice only, given that there were 32 different stimuli presented in all stimulus  
198 recordings in mice; macaque stimulus recordings included repeating the same checkerboard im-  
199 age), and (v) split-half  $r$  (Methods). We plotted EV against each of these variables (mouse: **Figure 6B**,  
200 macaque: **Figure 6E**) and report the correlation coefficient between EV and each variable in the y-  
201 axis in **Figure 6A** (mouse) and **Figure 6D** (macaque).

202 In mice, during both stimulus presentation and gray screen presentation, the most correlated  
203 property with a neuron's inter-areal predictability was the max  $r^2$  (**Figure 6A**). For the other 4 prop-  
204 erties, there was a strong distinction between stimulus presentation (dark bars) and gray screen  
205 presentation (light bars): All 4 properties were positively correlated with the neural activity pre-  
206 dictability EV fraction during stimulus presentation but they were slightly anticorrelated with their  
207 predictability EV fraction during gray screen presentation. Because the split-half correlation calcu-  
208 lation averages out the non-stimulus-dependent variability in both halves of the trials, it showed  
209 a weaker correlation with EV, which depends on trial-by-trial modulation. The one-vs-rest  $r^2$  met-  
210 ric, which also examines trial-by-trial modulation and does not average split-half trials, yielded a  
211 stronger correlation with EV.

212 When examining the relationship between 1-vs-rest self-consistency and inter-laminar predic-  
213 tion EV in mice, we observed a bimodal distribution of neurons: one group of neurons showed  
214 high EV despite having low self-consistency and in the other group EV correlated well with self-  
215 consistency (**Figure 6B** third column). The responses of neurons with low self-consistency also  
216 showed high EV during gray screen presentation. This bimodality was present in two out of the  
217 three mice we tested (MP031 and MP032; self-consistency and EV fraction relationships across all  
218 mice can be seen in **Figure Supplement 5A**). To better understand the responses of neurons with  
219 low self-consistency we projected out the "non-visual ongoing neuronal activity" from the neuronal  
220 responses (**Stringer et al., 2019a**) (Methods). This non-visual ongoing activity is deemed to be in-  
221 fluenced by spontaneous behavior (**Stringer et al., 2019b**). Projecting out this non-visual activity  
222 largely led to a unimodal distribution (**Figure 6C**). Removing the non-visual ongoing activity also in-  
223 creased the correlation between self-consistency and inter-laminar predictability (**Figure 6C**). This  
224 observation could be because the responses of neurons with low self-consistency can no longer be  
225 predicted, or because the responses of those neurons became more reliable and therefore were  
226 highly predicted. To distinguish between these two possibilities, we compared both the 1-vs-rest  
227 self consistency and the prediction EV before and after removing the non-visual activity. Removing  
228 the non-visual ongoing activity increased the self-consistency value across the three mice (**Figure**  
229 **Supplement 5C**;  $p < 0.001$ , paired permutation test). Interestingly, the inter-laminar EV fraction  
230 decreased in MP031 and MP032 mice, yet increased in MP033 (**Figure Supplement 5D**  $p < 0.001$ ,  
231 paired permutation test). When examining individual pairwise relationships in a fraction of highly  
232 predictable neurons, we found that some of the highly predictable neurons remained predictable  
233 after removing the non-visual activity whereas other highly predictable neurons dropped EV frac-  
234 tion dramatically.

235 In macaques, one of the highest correlated property with inter-areal prediction EV across all con-  
236 ditions was also the max correlation value (**Figure 6D**, E first column). Other neuron properties like  
237 SNR, split-half correlation and one-vs-rest correlation were also highly correlated with inter-cortical  
238 predictability EV (**Figure 6D**). Unlike the mouse, the split-half correlation was highly correlated with

239 EV fraction, although the relationship was highly non-linear (**Figure 6D**, middle column). Using the  
240 one-vs-rest squared correlation removed some of this non-linearity and further increased the cor-  
241 relation between it and the EV fraction (**Figure 6D**, third column). In addition, there was no bimodal  
242 distribution of neurons when relating one-vs-rest correlation and EV fraction.

243 We conjectured that neurons that have overlapping receptive fields (RFs) should share more  
244 information, and therefore their responses would better predict each other than neurons with  
245 non-overlapping RFs. In addition, even when all neurons are exposed to the same stimulus (full  
246 field symmetrical checkerboard image, gray screen, darkness, etc), neurons with overlapping RFs  
247 may be more synaptically connected, resulting in better inter-cortical predictions. To test this hy-  
248 pothesis, we compared inter-cortical predictions in different ensemble of neurons with RFs that  
249 differed in their degree of overlap. This hypothesis was only tested in the macaque data because  
250 we did not have access to RF estimates in the mouse data. For each V4 site whose responses we pre-  
251 dicted, we separated the predictors into two size controlled groups: one where all the V1 predictor  
252 sites had <10% RF overlap (sample of one V4 site, **Figure 6F**, top), and one where all the V1 pre-  
253 dictor sites had >80% RF overlap (sample of one V4 site, **Figure 6F**, bottom). A similar procedure  
254 was followed when predicting the activity of V1 neurons from V4 predictor neurons (**Figure 6H**).  
255 Inter-areal prediction was higher in the >80% RF overlap condition compared to the <10% RF over-  
256 lap ensembles in both directions and across all stimulus conditions (**Figure 6G,I**,  $n = 110$  total V4  
257 site recordings across all condition,  $n = 970$  total V1 site recordings across all conditions). In most  
258 cases, predicting the >80% RF overlap ensembles was still lower than ceiling performance (when  
259 using all predictors with all types of overlap percentages; **Figure 6E,F**)

### 260 **Inter-areal predictability is both stimulus and non-stimulus driven**

261 The results in **Figure 5** and **Figure 6** pointed to components of the predictable responses that  
262 are stimulus driven and other components that are non-stimulus driven. To further examine the  
263 non-stimulus driven component, we reasoned that if the shared information between areas were  
264 strictly driven by the visual stimulus, then using the activity of a stimulus presentation repeat to  
265 one specific image could be used to predict the responses to any other stimulus repeat of the  
266 same image. On the other hand, if the shared activity does not have any stimulus response infor-  
267 mation, then the prediction model would not work when considering responses across repeated  
268 presentation of identical stimuli in different trials. To test these two opposing ideas, we compared  
269 the inter-areal prediction EV fractions using unshuffled versus shuffled trials. Shuffling was done  
270 across repeat trials of the same images (mice: **Figure 7A**, macaques: **Figure 7D**). In mice, one stimu-  
271 lus presentation was either a drifting grating or a natural static image. In macaques, one stimulus  
272 presentation was either the one checkerboard image, a large thick fast moving bar, or a small  
273 thin slow moving bar. In both species and in both directions, inter-areal prediction EV fraction per-  
274 sisted ( $p < 0.001$ , paired permutation test of shuffled trials prediction vs. shuffled frames prediction),  
275 yet the EV fraction decreased after shuffling stimulus repeats compared to before shuffling (**Fig-  
276 ure 7B,E**). In mice, neurons showed a bimodal distribution in terms of their response predictability  
277 in shuffled and unshuffled trials. For a subset of neurons, the EV fraction was still high in the shuf-  
278 fled condition, albeit their EV was still higher in the unshuffled case (**Figure 7C**; points below but  
279 near the diagonal line). For another subset of neurons the EV fraction during shuffled trials was  
280 much lower or even near zero. The responses of the latter group had the highest predictability dur-  
281 ing gray screen activity. In the macaque, there was no bimodal distribution, yet neurons farther  
282 away from the diagonal line also had a higher EV fraction during gray screen activity (**Figure 7F**). In  
283 addition, we examined whether shuffling repeat presentations of gray screen images (simulating  
284 spontaneous activity) would result in any prediction at all. We found a more profound decrease in  
285 inter-cortical performance (**Figure Supplement 6B**) with no neurons that remained as predictable  
286 during shuffled repeats compared to unshuffled repeats (**Figure Supplement 6C,D**).

287 **Accounting for latency differences improves inter-areal activity predictions in**  
288 **macaque visual area sub-populations**

289 Given the latency differences in neuronal responses between V1 and V4 *Schmolesky et al., 1998*,  
290 we asked whether accounting for this latency could result in better inter-area prediction. To test  
291 this hypothesis, we offset the neuronal activity using different lags for each area (*Figure 7G, H*) and  
292 recalculated the ridge regression predictions. For each offset level, we calculated the percentage of  
293 neurons where the EV fraction peaked at that offset. For the checkerboard image, in the macaque  
294 V1→V4 predictions, the biggest percentage of neurons had a peak performance when there was  
295 no time offset between areas (*Figure 7I, left*). A substantial proportion of neurons had a peak  
296 performance for 25 ms or 50 ms offsets in the negative direction (i.e., V1 activity preceding V4  
297 activity). This distribution of peak EV values was only present during early visual responses (first 275  
298 ms of stimulus onset). In the macaque V4→V1 direction, there was a large proportion of neurons  
299 with peak EV when considering 25 ms to 50 ms offsets in the positive direction (i.e., V4 after V1,  
300 *Figure 7I, right*). These differences were apparent in the early part of the visual response, before  
301 250 ms. When offsetting the neuronal responses to gray screen presentations, across all times and  
302 areas, the highest percentage of neurons with peak EV was when there was no time offset (*Figure*  
303 *Supplement 6E,F*).

304 **Discussion**

305 Neuronal activity in one brain region or layer within the visual cortex can be used to predict neu-  
306 ron activity in another nearby and anatomically connected region or layer in single trials (*Fig-  
307 ure 2*). In monkeys, predictability was asymmetric: V1 activity better accounted for V4 activity than  
308 vice versa (*Figure 3, Figure 7*). This inter-areal prediction persisted across different stimuli (*Figure 4*)  
309 but also in the absence of a visual stimulus, during gray-screen and lights-off periods (*Figure 5*). The  
310 degree of predictability increased with signal-to-noise ratio, response variance, and the degree of  
311 overlap between receptive fields (*Figure 6*).

312 In line with other studies in mice (*Stringer et al., 2019b; Niell and Stryker, 2008; Andermann*  
313 *et al., 2011*), we observed an approximately bimodal distribution of neuronal responses, with a  
314 large subset of neurons that do not show reliable responses to visual stimuli both in L4 and L2/3.  
315 Yet, even if these neurons are “non-visual”, at least within the set of stimuli and conditions ex-  
316 amined here, their activity remains highly predictable. This bimodal distribution dissipates when  
317 projecting out potential non-sensory ongoing activity (*Stringer et al., 2019b, 2021*). At the popu-  
318 lation level, neuronal encoding subspaces in mouse visual cortex have been shown to have little  
319 overlap between visual sensory and non-sensory (behavioral) information, with only one shared  
320 dimension (*Stringer et al., 2019b*). The visually unreliable, yet highly predictable, subset of neurons  
321 described here could be the neuronal group driving this orthogonality. As expected, the activity  
322 of “visual” neurons can be better predicted during visual presentation and is predicted almost at  
323 chance levels during gray screen presentation. In stark contrast, the activity of non-visual neurons  
324 can be predicted even better during gray screen presentation than during visual stimulation. There  
325 was no such bimodal distribution in the data from monkeys. One possibility is that there may be  
326 no (or very few) non-visual neurons in macaque V1 or V4. Indeed the overwhelming majority of  
327 neurons in V1 and V4 responded strongly to visual stimulation. Yet, the comparisons between the  
328 results in mice and monkeys reported here need to be interpreted with caution because the two  
329 datasets differ in terms of recording techniques (electrophysiology versus two-photon imaging),  
330 consequently also the temporal resolution (one millisecond versus hundreds of milliseconds), and  
331 the type of interaction studied (across areas versus across layers), in addition to any differences  
332 between species.

333 In macaques, sites where the receptive fields (RF) of V1 and V4 overlap can better predict  
334 each other compared to other sites showing little RF overlap. This observation could reflect RF-  
335 dependent intrinsic connectivity between areas, but also RF-dependent shared inputs from other

336 areas like the thalamus. In the latter case, those putative shared inputs cannot be strictly depen-  
337 dent on visual inputs given that the effect of RF overlap persists even during gray screen conditions.

338 Many computational models that aim to explain neuronal activity in visual cortex are based on  
339 feedforward signal propagation, with increased receptive field sizes, selectivity, and feature invari-  
340 ance along the visual hierarchy (*Serre et al., 2007b; Kreiman, 2021; Connor et al., 2007*). Consistent  
341 with this idea, we described an asymmetry in the degree of predictability, with V1 neurons explain-  
342 ing V4 responses better than the other way around. This observation persisted after controlling for  
343 neuronal count and split-half correlation values and was also apparent during the lights-off condi-  
344 tion. In contrast, there was no asymmetry when comparing inter-laminar prediction directions  
345 in mice. The lack of asymmetry in inter-laminar prediction directions in mice could be due to the  
346 slow dynamics in calcium imaging, the lack of a clear inter-areal hierarchy, or differences between  
347 species.

348 The asymmetry in directionality is also observed when implementing temporal delays to inter-  
349 areal prediction, consistent with processing delays across areas (*Semedo et al., 2022; Gokcen et al.,*  
350 *2022; Schmolesky et al., 1998*). A substantial proportion of neurons increased their inter-areal  
351 predictability when offsetting the times between areas, specifically in the direction that aligns their  
352 neuronal activities. In contrast to the temporal delays associated with processing visual stimulation,  
353 during gray screen presentation, the majority of neurons was best predicted in the absence of  
354 any time offsets, suggesting that the internally generated neuronal activity during spontaneous  
355 conditions may be largely driven in a non-feedforward manner.

356 Further evidence supporting the distinction between visually-driven and non-visually-driven in-  
357 teractions comes from the observation that trial repeat shuffling reduced, but did not eliminate,  
358 predictability in both mice and monkeys. In mice, when plotting shuffled vs. unshuffled activity,  
359 we encountered again a bimodal distribution, where a group of neurons was closer to the diagon-  
360 al line (their responses were predicted as well during the shuffled compared to the non-shuffled  
361 condition), and another group of neurons which were closer to the x-axis (their responses could  
362 not be predicted during the shuffled condition). The responses of the latter group were best pre-  
363 dicted during gray screen activity, suggesting that they mostly shared non-visual information. The  
364 predictive power in mouse V1 from layer 4 to layer 2/3 during spontaneous conditions has been  
365 recently shown in (*Papadopouli et al., 2024*), consistent with our findings. The overall area popula-  
366 tion decrease in predictability after shuffling may be due to the influence of non-visual activity such  
367 as movement (*Stringer et al., 2019b*), especially since these non-visual stimulus effects have been  
368 shown to occur in the one-second timescale as in our study. In the macaque, context-dependent  
369 effects are likely not due to movement, since the monkey maintained fixation during the stimulus  
370 task, and visually-evoked activity is not driven by movement (*Talluri et al., 2023*).

371 The results on the prediction of neuronal responses constitute a lower bound. First, we focus  
372 on linear predictability but other (non-linear) models could better capture neuronal activity. Sec-  
373 ond, and critically, the experimental data provide only a fraction of the inputs to a given neuron—  
374 excluding most (in macaque dataset) if not all (in mouse dataset) inhibitory inputs that are crucial  
375 for the organization of circuit and microcircuits in visual cortex (*Jiang et al., 2015; Shen et al., 2020;*  
376 *Ibrahim et al., 2020; Schuman et al., 2021*). Third, biophysical realistic models of the transforma-  
377 tion between inputs and outputs of a given neuron should include their dendritic locations and  
378 specific synaptic potentials (*Park et al., 2019; Petousakis et al., 2023*).

379 We introduce a unifying method to evaluate inter-areal interactions in different types of neu-  
380 ronal recordings, timescales, and species. These interactions can be assessed in single trials, sep-  
381 arating visually-driven and non-visual contributions, and accounting for the directionality and dy-  
382 namics of neuronal responses. These efforts constitute an initial step towards systematically build-  
383 ing computational models that can account for the transformations from sensory inputs to their  
384 encoding in the cortex.

## 385 Methods

386 **Datasets.** We used the mouse dataset from (*Stringer et al., 2019a*) containing calcium-imaging  
387 activity measurements from 43,630 neurons in layer 4 (L4) and 12,060 neurons in layers 2/3 (L2/3)  
388 in V1 of 4 mice during 32 different randomly interleaved presentations of either drifting gratings  
389 or gray-scale natural images (each one repeated more than 90 times), along with spontaneous ac-  
390 tivity during 30 minutes of exposure to a gray/black screen (*Figure 1A*, data acquisition details in  
391 (*Stringer et al., 2019a,b*)). Calcium imaging activity was recorded during stimulus presentations at  
392 a scan rate of 2.5 Hz or 3 Hz (each frame was acquired every 400 ms or 333 ms). The computed  
393 stimulus responses per stimulus presentation were averaged based on two frames immediately  
394 post stimulus onset. Cortical layers were determined using the 10-12 planar z-positions retrieved  
395 during the multi-plane calcium activity acquisition. For stimulus-response and spontaneous record-  
396 ings, neuronal activity of each neuron was z-scored using its 30-minute gray screen spontaneous  
397 activity (mean gray-screen activity subtracted and divided by gray-screen activity standard devia-  
398 tion).

399 We used the macaque monkey dataset from (*Chen et al., 2022*). This dataset consists of en-  
400 velope multiunit activity (MUAe) from 1,024 recording sites in one monkey in response to either  
401 multiple-day recordings of more than 60 repetitions of a full-size checkerboard image, moving  
402 small-thin or large-thick bars in 4 directions, gray screen presentations, or more than 30 minutes  
403 of baseline activity where the monkey was in a room with the lights off (*Figure 1B*). Neuronal ac-  
404 tivity was averaged over 25 ms non-overlapping bins. Activity duration was 300 ms, 400 ms, and  
405 1 s for gray screen, checkerboard, and moving bar presentations, respectively. For the recordings  
406 during visual stimulation, the neuronal activity was normalized by subtracting the mean activity  
407 during the gray screen presentations separately for each site.

408 **Visual responsiveness.** A neuron or site was defined to be visually responsive if its signal-to-noise  
409 ratio (SNR) was 2 or higher and its split-half correlation value was 0.8 or higher. Due to the high  
410 number of repetitions of visual stimuli, the split-half correlation was skewed toward high values,  
411 which is why we used a higher split-half correlation threshold than commonly used in other studies.  
412 In mice, the SNR for each neuron was calculated as:

$$SNR_{mouse} = \frac{\langle r_{stim} \rangle - \langle r_{spont} \rangle}{std(r_{spont})} \quad (1)$$

413 where  $\langle \rangle$  denotes mean,  $std$  denotes the standard deviation,  $r_{stim}$  is the average activity in response  
414 to stimuli, and  $r_{spont}$  indicates the average activity over the 30-minute gray screen presentation  
415 activity.

416 In monkeys, we followed the definition in (*Chen et al., 2022*) and calculated the SNR for each  
417 site as:

$$SNR_{monkey} = \frac{\max(\langle r_{stim} \rangle) - \langle r_{spont} \rangle}{std(r_{spont})} \quad (2)$$

418 using the peak activity during the checkerboard presentation for the signal, and the average gray  
419 screen neuronal activity as background (denoted as  $r_{spont}$ ).

420 In mice, the split-half consistency was calculated by correlating the average activity for the 32  
421 stimuli in a randomly chosen half of the trials, with the average activity in the other half of the trials,  
422 followed by Spearman-Brown correction (used to correct for the division of trials by half). In mon-  
423 keys, during checkerboard presentations, the split-half consistency was calculated by correlating  
424 the average activity of the 16 timepoints (0–400 ms; 25 ms bins) of checkerboard presentation of  
425 25 random trial repetitions with the average activity of another non-overlapping 25 random rep-  
426 etitions, followed by Spearman-Brown correction. During moving bar presentations, the 40 time-  
427 points (0–1s; 25 ms bins) during 25 random trial repetitions were first concatenated across the 4  
428 directions (total of 160 timepoints), and then correlated to the concatenated averaged activity of  
429 another nonoverlapping 25 random trial repetitions, followed by Spearman-Brown correction. For  
430 all split-half consistency calculations, we randomly sampled trials 20 times.

431 **Inter-areal regression.** Let  ${}_A r_{i,t}$  be the activity of neuron or site  $i$  in area  $A$  at timepoint  $t$ , where  $A$   
432 can be L4 or L2/3 in the mouse data and V1 or V4 in the monkey data. Neuronal activity from one  
433 area (e.g., mouse V1 L4 or macaque V1) was used to predict activity in the other area (e.g., mouse  
434 V1 L2/3 or macaque V4) using ridge regression (**Figure 1E**). The activity of each neuron  $i$  in area  $A_2$   
435 was predicted from  $n_{A_1}$  neurons in area  $A_1$  as follows:

$${}_{A_2} \hat{r}_{i,t} = \sum_{j=1}^{n_{A_1}} w_{i,j} {}_{A_1} r_{j,t} + b_i \quad (3)$$

436 During fitting, we minimized the residual sum of squares (RSS), defined as:

$$RSS_i(\mathbf{w}, b_i) = \sum_{t=1}^{n_T} ({}_{A_2} \hat{r}_{i,t} - {}_{A_2} r_{i,t})^2 + \alpha \sum_{j=1}^{n_{A_1}} w_j^2 \quad (4)$$

437 where  $\mathbf{w}$  is the weight vector for predicting the activity of neuron  $i$ ,  $n_T$  is the number of images/time  
438 points and  $\alpha$  controls the regularization strength ( $\alpha$  was tuned for each dataset with an indepen-  
439 dent sample and ranged from  $10^3$  to  $10^5$ ). Predictability for each neuron was evaluated using 10-  
440 fold cross-validation across trials and quantified as squared Pearson's  $r$ , referred to as explained  
441 variance fraction (EV fraction) throughout.

442 To remove temporal auto-correlation that would inflate the apparent prediction despite cross-  
443 validation, we removed training timepoints near the test timepoints closer than the decay window  
444 of the activity auto-correlation (mouse: 5 s; macaque: 1.5 s). The auto-correlation decay window  
445 was determined using time-series forecasting Ridge Regression (using  $r_i$  to predict  $r_{i+d}$ , where  $d$   
446 represents a delay). The delay was increased until the EV fraction approached chance.

447 **Prediction directionality.** We compared predictability across layers in different directions (in  
448 mice: L4→L2/3 vs. L2/3→L4) and also predictability across areas in different directions (in  
449 macaques: V1→V4 vs. V4→V1) (**Figure 3**). To ensure that results were not dependent on the num-  
450 ber of neurons/sites, we randomly subsampled the number of neurons/sites of the area contain-  
451 ing the larger number of neurons/sites (L2/3 for mouse; V1 for macaques) to match the number  
452 of predictors in both directions (10 permutations, neuron count details in **Table 1** and **Table 2**). To  
453 account for potential changes in intrinsic predictability, we ensured that the neurons from both ar-  
454 eas were matched in terms of the distribution of split-half correlation values so that the difference  
455 between individual area neurons/sites was less than 0.002. To assess the intrinsic predictability of  
456 neurons/sites in each region, the areas were used to predict themselves, where one neuron/site  
457 in the area was predicted by the remaining neurons in the same area. This “intra-areal” prediction  
458 was used to normalize EV fraction to compare directionality of prediction.

459 **Stimulus types and spontaneous activity comparison.** We compared predictability for different  
460 stimulus conditions (**Figure 4, Figure 5**). To compare inter-areal prediction across stimulus types  
461 and between the presence or absence of stimuli, the number of predictors (neurons or sites) and  
462 timepoints was sub-sampled to be the same across all datasets. In the macaque, the time spent  
463 recording the lights-off condition was much greater than during stimulus or gray screen presenta-  
464 tions. To account for the difference in time duration and therefore training size, we subsampled  
465 time periods to be the same across all stimulus, gray-screen, and lights-off, lights-off eyes open,  
466 and lights-off eyes closed conditions.

467 **Neuron properties.** We compared different neuronal properties with predictability measure-  
468 ments (**Figure 6**). The SNR and split-half correlation has been defined above. The absolute max  
469 pairwise correlation value of each neuron/site  $i$  in one area with all neurons in the other area was  
470 calculated as

$${}_{A_2} \text{maxcorr}_i = \max_j (|\text{corr}({}_{A_2} r_i, {}_{A_1} r_j)|) \quad (5)$$

471 where  ${}_{A_2} r_i$  represents the activity of neuron/site  $i$  in area  $A_2$ , which are correlated with the activity  
472 of every neuron  $j$  in area  $A_1$  (denoted as  ${}_{A_1} r_j$ ).

473 The one-vs-rest correlation was calculated as follows. In the mouse data, we correlated the  
474 activity for the 32 stimuli during 1 trial repetition with the averaged activity of the remaining trial

475 repetitions. In monkey, during checkerboard presentations, the one-vs-rest correlation was calcu-  
476 lated by correlating the activity of the 16 timepoints (0–400 ms; 25 ms bins) during 1 trial repetition  
477 with the averaged activity of the remaining trial repetitions. For moving bar presentations, the 40  
478 timepoints (0–1s; 25 ms bins) during 1 trial repetition were first concatenated across the 4 direc-  
479 tions (total of 160 timepoints), and then correlated to the concatenated, trial-averaged activity of  
480 the remaining trial repetitions. For all one-vs-rest correlation calculations, we held out each trial in  
481 turn and averaged across the samples.

482 **Receptive field overlap comparisons.** In macaque, receptive field (RF) ellipses were calculated  
483 using center and edge locations in the dataset (*Figure 6E, F*). To calculate the percentage of RF over-  
484 lap between the neuronal sites to be predicted and the predictor, the intersection area between  
485 ellipses was retrieved using the Shapely python package, and divided by the area of the predicted  
486 site. Sites that had predictors that overlap both more than 80% and less than 10% were selected  
487 to compare inter-areal predictions. To control for predictor size, 14 random predictor sites from  
488 all the sites in each overlap type were subsampled (10 random samples without replacement).

489 **Trial repeat shuffling and time offset predictions.** For the shuffled-trial experiments, we shuf-  
490 fled the predictor activity across repeat trials showing the same stimulus (*Figure 7*). (Thus, the  
491 stimulus order remained the same.) For the mouse time-offset analysis, the activity of predictor  
492 neurons was time-shifted in the positive or negative direction, with 1 bin corresponding to 1 stimu-  
493 lus presentation (800–900ms). For the monkey dataset, the predictor activity (400 or 1000 ms per  
494 presentation, 16–50 bins of 25 ms each) was offset across time bins. We used sub-windows of 200  
495 ms to avoid window-length differences that would otherwise be introduced if we shifted the entire  
496 trial response.

497 **Data and code availability.** All the computational models and data analysis code developed in  
498 this work is publicly available at this link: <https://github.com/4sdch/inter-area-neural-prediction.git>.  
499 All the data are publicly available for mouse: [https://figshare.com/articles/dataset/Recordings\\_of\\_](https://figshare.com/articles/dataset/Recordings_of_ten_thousand_neurons_in_visual_cortex_in_response_to_2_800_natural_images/6845348?file=12462734)  
500 [ten\\_thousand\\_neurons\\_in\\_visual\\_cortex\\_in\\_response\\_to\\_2\\_800\\_natural\\_images/6845348?file=](https://figshare.com/articles/dataset/Recordings_of_ten_thousand_neurons_in_visual_cortex_in_response_to_2_800_natural_images/6845348?file=12462734)  
501 [12462734](https://figshare.com/articles/dataset/Recordings_of_ten_thousand_neurons_in_visual_cortex_in_response_to_2_800_natural_images/6845348?file=12462734) (*Stringer et al., 2019a*) and for macaques: [https://gin.g-node.org/NIN/V1\\_V4\\_1024\\_](https://gin.g-node.org/NIN/V1_V4_1024_electrode_resting_state_data)  
502 [electrode\\_resting\\_state\\_data](https://gin.g-node.org/NIN/V1_V4_1024_electrode_resting_state_data) (*Chen et al., 2022*).

Figures and Tables 503

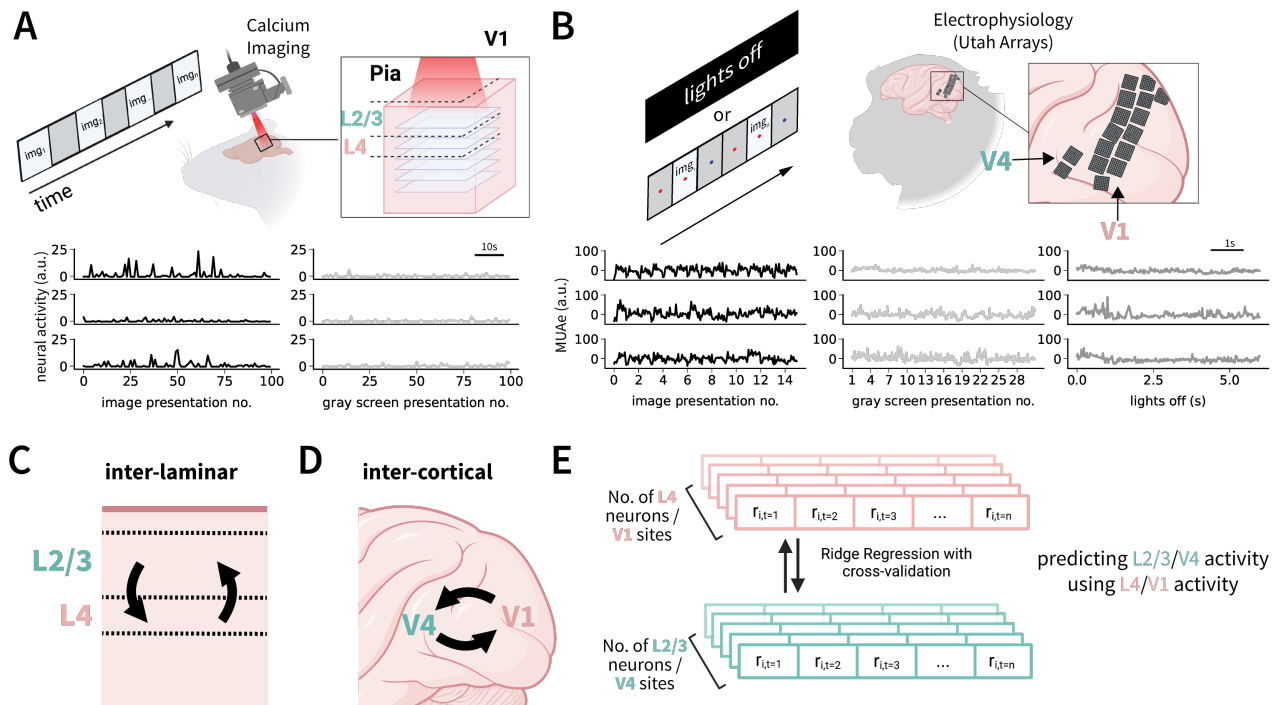


**Figure 1. Predicting trial-to-trial and timepoint-to-timepoint neuronal activity between areas.** **A.** Top: Experimental set-up to record two-photon Calcium imaging activity data from layers 2/3 (L2/3) and layer 4 (L4) in rodent V1 upon presentation of gratings, natural stimuli or gray screen images (represented as  $img_n$ ) (Stringer et al., 2019a). Deconvolved calcium imaging traces were z-scored using baseline activity during 30 minutes of gray screen presentation before/after image presentation (Table 1). Bottom: Sample z-scored neuronal activity from 3 different neurons in response to 100 presentations of drifting gratings (left) or gray screen presentations (right). Each activity value corresponds to one image presentation, and calculated as the average of two calcium imaging video frames (666 ms or 800 ms, see details in Methods). **B.** Top: Experimental set-up for the neuronal activity data from macaque V1 and V4 (Chen et al., 2022). Electrophysiological activity was simultaneously recorded across 1,024 channels from 16 Utah arrays (Table 2). Bottom: Envelope multiunit spiking activity (MUAe) from 3 different sites in response to multiple presentations of a repeated 400 ms full-field checkerboard image (left, baseline mean-subtracted), 200 ms gray screen (middle), or during a lights-off condition (30 minutes total; right). Each value corresponds to aggregated MUAe activity in a 25 ms bin. **C.** Overview of inter-laminar relationships examined in mouse V1. “lower-level” layer 4 (L4) neuronal activity is used to predict “higher level” layer 2/3 (L2/3) activity (blue arrow) and vice versa (red arrow). **D.** Overview of inter-cortical relationships examined in macaque, where lower-level V1 is used to predict higher-level V4 (blue arrow) and vice versa (red arrow). **E.** Illustration of linear ridge regression method used for inter-areal prediction. Neuronal activity in response to presentation number  $i$  (labeled “ $r_i$ ”) at time  $t$  from one area (e.g., mouse V1 L2/3 or macaque V1) was used to predict activity in the other area (e.g., mouse V1 L4 or macaque V4) (Semedo et al., 2019). Predictability was evaluated using 10-fold cross-validation across presentation trials in mouse, and across 25 ms timepoints in macaque (Methods).

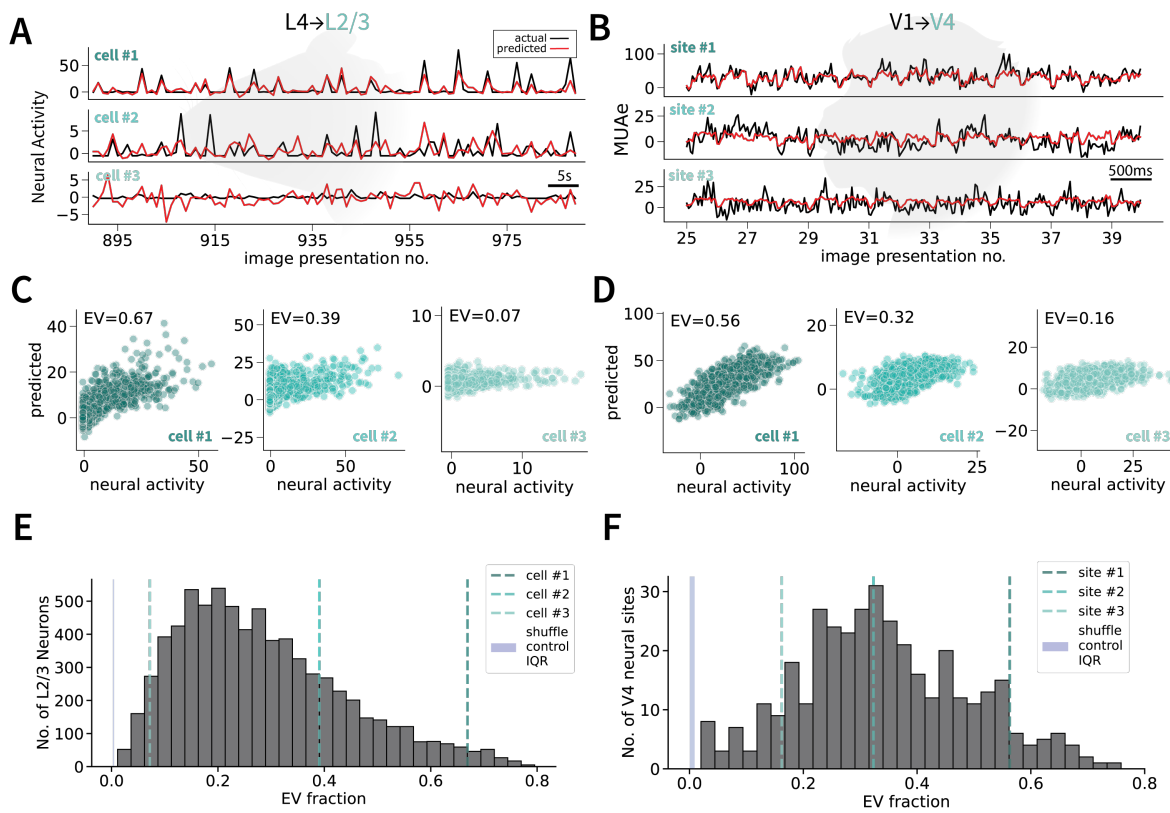


**Figure 2. Lower level activity can predict higher level activity in both rodent and primate brains.** **A.** Example neuronal activity (z-scored, black) in response to stimulus presentations (drifting gratings) in mouse V1 L2/3 along with regression-model predictions (red) for a typical cell (2, middle), cell in the top 10% percentile of predictability (1, top), and bottom 10% percentile (3, bottom). **B.** Same as **A** for macaque MUAe activity in response to a full-field checkerboard image in three V4 neuronal sites. **C.** Predicted neuronal activity versus actual neuronal activity in response to stimuli for the mouse L2/3 cells 1, 2, and 3 shown in **A**. Each point represents 800 ms corresponding to a stimulus presentation.  $r$  values (top left) indicate the correlation coefficient. **D.** Same as **C** for macaque V4 neuronal sites 1, 2, and 3. Each point represents one 25ms timepoint during the 400 ms presentation. **E.** Distribution of EV fraction in L4→L2/3 regressions of neuronal activity in response to visual stimuli in cells that were deemed visually responsive in 4 mice and 7 recording days ( $n = 7,265$  neurons, *Methods*). Performance using 10-fold cross-validation across trials was quantified as squared Pearson's  $r$ , referred to as explained variance (EV) fraction. The three vertical lines show the 3 examples in part **A**, **C**. The blue solid shaded rectangle (here and throughout) represents the interquartile range (IQR) shuffle control performance, where the activity timepoints of one area were randomly shuffled. **F.** Distribution of EV fraction in V1→V4 regressions of neuronal activity in response to visual stimuli in sites deemed visually responsive (One macaque, 5 recording days, 68–82 V4 sites recorded per day;  $n = 376$  total site recordings).

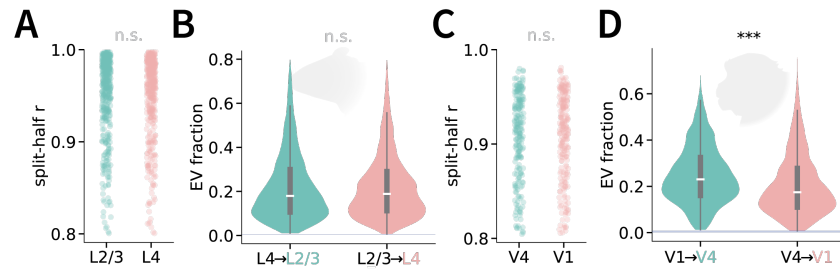


**Figure 3. Asymmetry in inter-cortical predictability in macaque but not inter-laminar predictability in mouse.** **A.** Split-half reliability (Methods) for the  $n = 298$  neurons (per area) in mouse MP033 drifting gratings presentation recording of V1 L2/3 (green) and L4 (coral) used to perform directionality comparisons. Neurons were randomly sub-sampled to match the numbers and self-reliability in the two distributions. Here and throughout, asterisks indicate statistically significant differences using a hierarchical independent permutation test (10,000 permutations): \*  $p < 0.05$ , \*\*  $p < 0.01$ , \*\*\*  $p < 0.001$ ; “n.s.” indicates  $p > 0.05$ . **B.** Violin plots describing the distribution of EV fraction for L4→L2/3 (green) and L2/3→L4 (coral) predictions across all 7 stimulus recordings ( $n = 1, 113$  neurons per area). Violin plots (here and throughout) represent the distribution of neuron/site values, with width representing density and inner boxplot representing the interquartile range. Whiskers of innerbox represent range of the data. **C.** Split-half reliability for the  $n = 74$  sites (per area) in macaque checkerboard recording (date=090817) of V4 (green) and V1 (coral) used to perform directionality comparisons. **D.** Violin plots describing the distribution of EV fraction for V1→V4 (green) and V4→V1 (coral) across all 5 stimulus recordings ( $n = 786$  sites recordings per area).

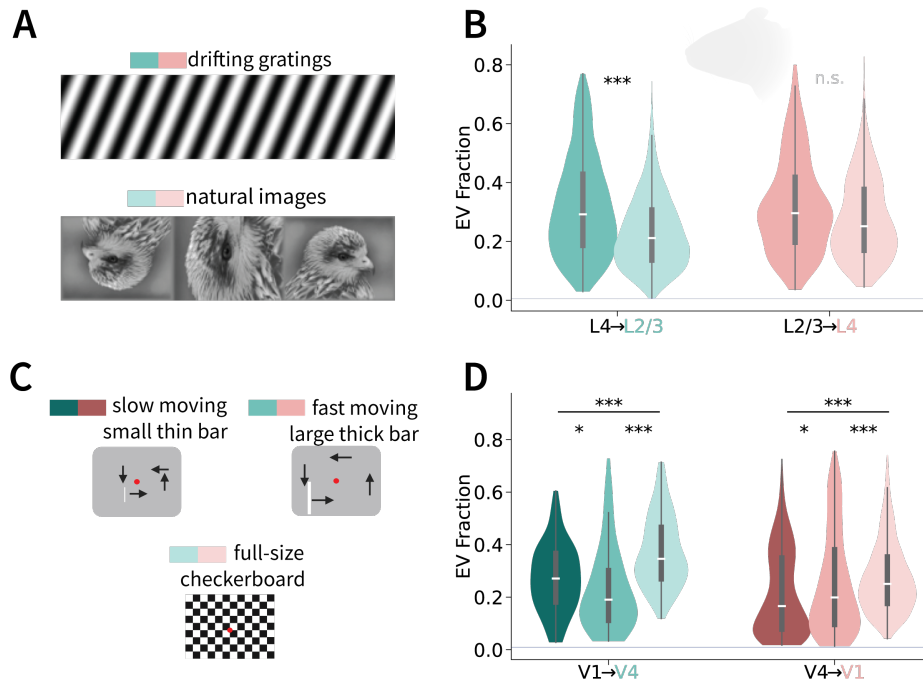


**Figure 4. Stimulus type influences neuronal predictability.** **A.** Illustration of the two types of stimuli (drifting gratings and static natural images) presented to the mouse during calcium imaging. **B.** Across-layer predictability in mouse V1 for each stimulus type (dark: drifting gratings, light: natural images) and prediction direction. **C.** Illustration of the three types of stimuli presented to the monkeys (*Chen et al., 2022*). The slow-moving small thin bar moved near the fixation point for 1 s in each of the four directions, while the fast moving large thick bar moved towards the edges of the screen for 1 s in each of the four directions. The full-field checkerboard image was presented repeatedly (400 ms each presentation). **D.** Across-area predictability for each stimulus type (dark: slow bars, medium: fast bars, light: checkerboard) and direction.

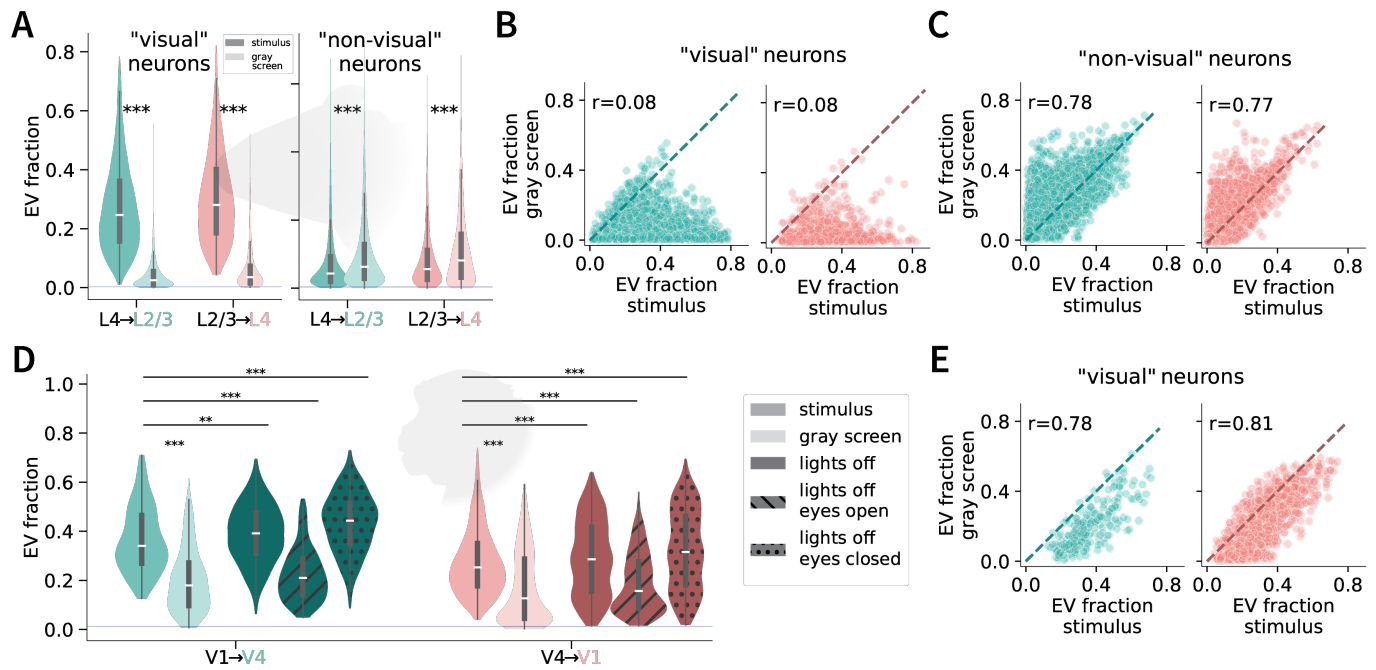


**Figure 5. Spontaneous activity can also be predicted.** **A.** EV fraction of neuronal activity in response stimulus presentation (dark violins) or gray screen presentation (light violins) for neurons deemed visually (left) or non-visually (right) responsive (Methods). **B.** Correlation between EV in responses to gray screen (y-axis) versus stimulus presentation (x-axis) in mouse V1 visually responsive neurons (L4→L2/3:left, green; L2/3→L4: right, coral). Diagonal line represents the line of equality ( $y=x$ ).  $r$  is the Pearson's  $r$  coefficient. **C.** Same as B but for non-visually responsive neurons. **D.** EV during stimulus presentations (checkerboard image, green), gray screen presentations (light green) or during lights off (dark green). The lights-off condition is further separated into periods when the eyes were open or closed. All lights-off conditions were sub-sampled (10 permutations) to contain similar training lengths as the stimulus and gray screen presentation recordings. **E.** Correlation between EV in responses to gray screen (y-axis) versus stimulus presentation (x-axis) in macaque visually responsive neurons (V1→V4:left, green; V4→V1: right, coral). Diagonal line represents the line of equality ( $y=x$ ).  $r$  is the Pearson's  $r$  coefficient. All recorded sites were pulled from the 3 recording days of checkerboard presentations.

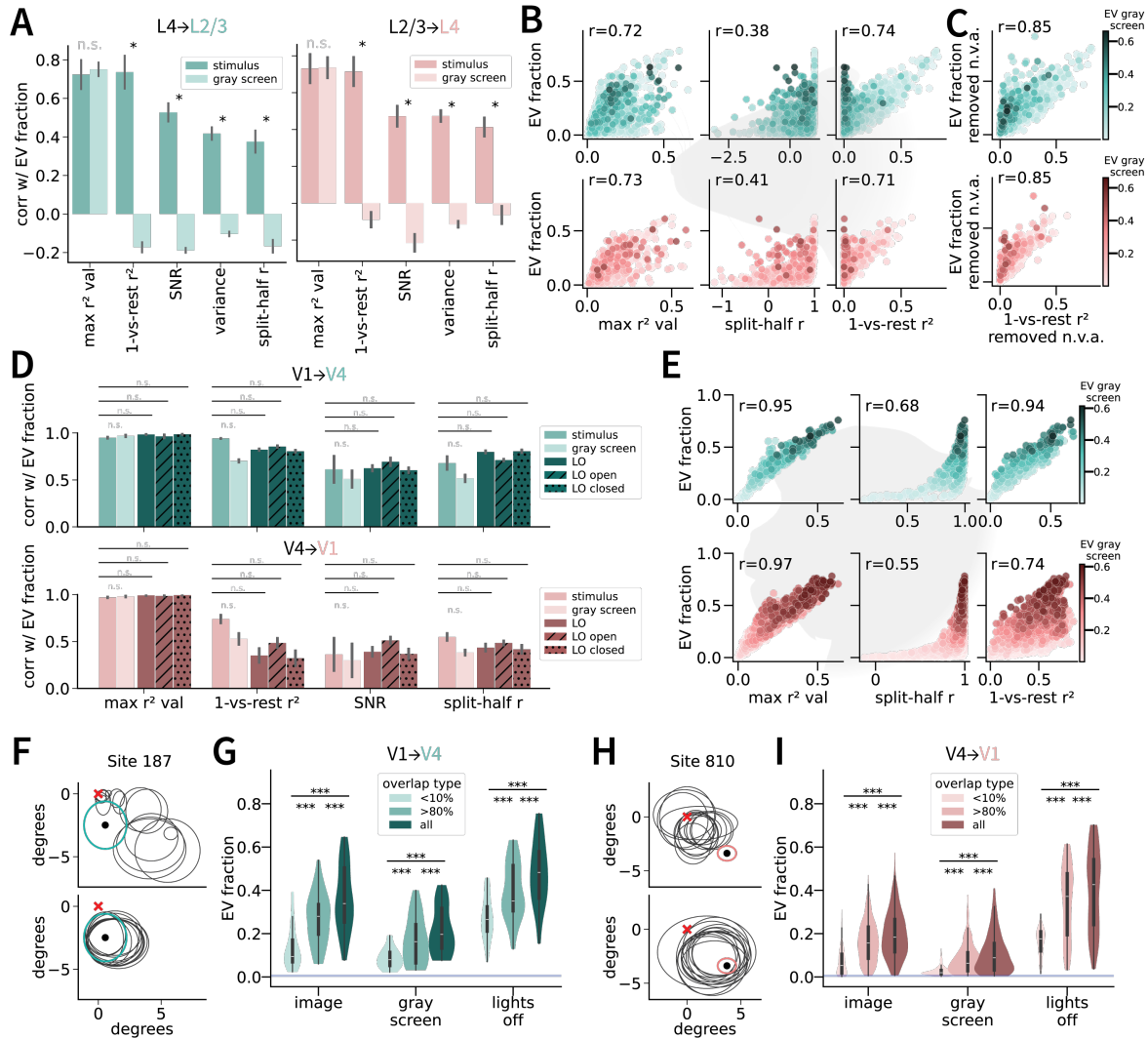


**Figure 6. neuronal predictability depends on SNR, stimulus response variance, and receptive field overlap.** **A.** Correlation between different neuronal properties with the predictability of L2/3 (green) and L4 (coral) neuronal responses during the presence (dark color) or absence (light color) of visual stimulus. Neuronal properties measured in mouse L2/3 and L4 include the correlation value of the most correlated pair to each cell (max correlation value, squared), a modified metric of self-consistency (one-vs-rest correlation, squared), SNR, variance in the neuronal activity in response to different stimuli, and the traditional metric of self-consistency (split-half correlation  $r$ ) (Methods). **B.** Relationship between three neuronal properties and their predictability in a randomly chosen sub-sample of neurons ( $n = 4,000$ ) for mouse L2/3 (green) and L4 (coral) neuronal responses from both drifting gratings and natural images conditions (combined). Hue represents the degree of predictability for the same neurons during the 30 minutes of gray screen presentation (see color map on bottom right). **C.** 1-vs-rest square correlation relationship with predictability after projecting out dimensions of “non-visual” activity (using gray screen activity (Stringer et al., 2019a)). **D.** Correlation between different neuronal properties with the predictability of monkey V4 (green) and V1 (coral) neuronal site recordings during the full-field checkerboard presentation (dark color), gray screen presentation (light color), and lights-off condition (darkest color; solid, hatch lines, and hatch dots). Neuronal properties measured in the macaque visual cortex include the max correlation squared value, one-vs-rest squared correlation, SNR, and split-half correlation  $r$ . **E.** Same as **B** for the macaque V1 and V4 neuronal sites. **F.** Top: Receptive fields of one sample V4 neuronal site (green circle, array 2 electrode 187) and 14 randomly selected V1 neuronal sites as predictors (black circles), constrained on sites that share less than 10% receptive field overlap with the V4 site. Bottom: Receptive fields of the same neuronal site 187 and 14 randomly selected V1 neuronal sites used as predictors, constrained on sites that share at least 80% receptive field overlap with the V4 site. **G.** Differences in predictability of V4 neural activity ( $n = 110$  site recordings) in terms of 14 V1 predictor sites with less than 10% RF overlap (light green), 14 predictor sites with at least 80% RF overlap (green), and all predictors (dark green). Predictions were computed for recordings in response to the stimulus presentation (sliding bars and full-field checkerboard images), gray screen presentation, and lights off. **H.** Bottom and top left: Same as **F** but for macaque sample V1 site 810. **I.** Same as **D**, but for V1 ( $n = 970$  site recordings).

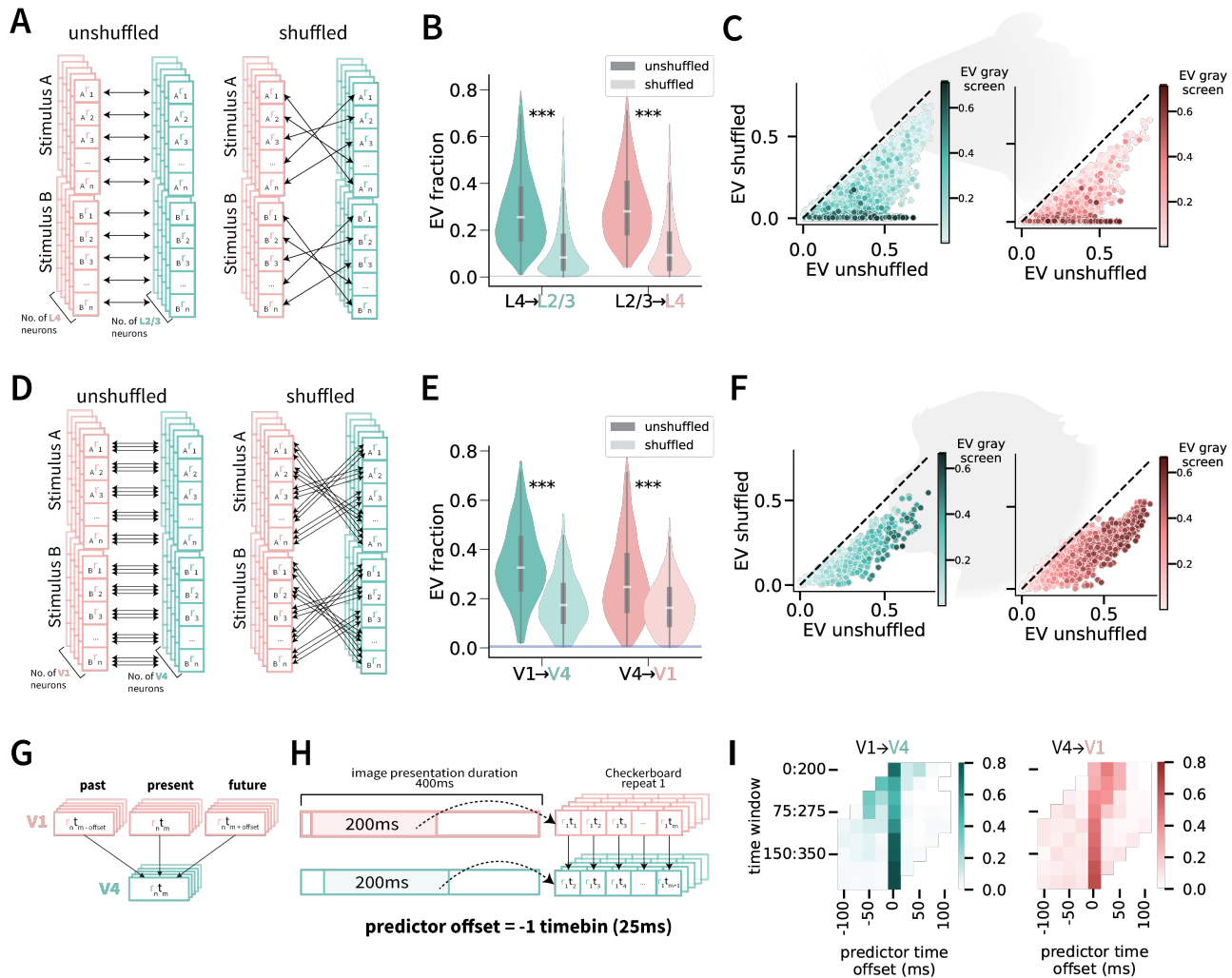


**Figure 7. Predicting neuronal activity across time reveals shared stimulus- and non-stimulus driven information in both mouse and macaque visual cortex, along with latency and non-latency specific correlations in macaque V1/V4.** **A.** Shuffled-trial-repeat experiment set-up for comparing unshuffled vs. shuffled prediction in mouse V1 L2/3 and L4. Neuronal activity in response to stimulus repeats was shuffled within their respective image. **B.** EV fraction for unshuffled (dark) and shuffled (light) trials in the L4 → L2/3 (green) and L2/3 → L4 (coral) directions. **C.** Relationship between shuffled (y-axis) and unshuffled (x-axis) trial repeat EVs in the mouse L4 → L2/3 (left, green) and L2/3 → L4 (right, coral) directions. Hue represents EV fraction during gray screen activity. **D.** Shuffled-trial-repeat experiment set-up comparing unshuffled vs. shuffled prediction in macaque data. Neuronal activity (including all timepoints) in response to stimulus repeats were shuffled within their respective image. Since checkerboard presentation was only one stimulus, visualization of experiment only applies to the “Stimulus A” portion. **E.** Same as **B** for macaque V1 → V4 (green) and V4 → V1 (coral). **F.** Same as **C** for macaque V1 → V4 (green) and V4 → V1 (coral). **G.** Illustration of time offsets applied to macaque neuronal activity for inter-areal predictions. Instead of neuronal activity prediction between areas being done on simultaneous activity (middle coral and bottom green box), the V4 neuronal activity (green) at time  $t_m$  was predicted using V1 neuronal activity (coral) at time  $t_{m \pm \text{offset}}$ . *offset* represents 1–8 timebins (25 ms per timebin) before (if negative; left coral box) or after (if positive; right coral box) time  $t_m$ . Time offset experiment was done in both prediction directions (V1 → V4 and V4 → V1). **H.** Experimental set-up example for predicting neuronal activity in V4 using V1 neuronal activity from 25 ms prior to V4 activity. Neural activity is in response to a repeated checkerboard image. A 200 ms section of the cortical area was used to represent the image presentation response, and was offset -1 timebin (25 ms) to predict a 200 ms target cortical area. During the prediction experiments, the 200 ms window was slid across the entire duration of the stimulus **I.** Time offset prediction results across both V1 → V4 (left, green) and V4 → V1 (right, coral) prediction directions. Each square corresponds to the fraction of neuronal sites whose neural activity were best predicted during that offset period and time window.

**Table 1.** Mouse neuron counts used for inter-layer prediction and analyses. A total of 7 recordings were used to perform prediction experiments. Each row corresponds to a recording day, containing the dataset recording type (Mouse Dataset), total number of neurons, and visually responsive neurons (see [Methods](#)). Fourth column: In the directionality prediction experiments, the area containing more neurons (L2/3) was further subsampled to match the number of L4 neurons. The dataset recording type names contain either “ori32” or “nating32”, in addition to the mouse name (MP0-). “nating32” represents dataset of the 32 natural image presentation. “ori32” represents dataset of the 32 drifting gratings.

Mouse Dataset	Layer 2/3			Layer 4	
	Total	visually responsive	Subsampled (directionality)	Total	visually responsive
nating32 MP031	6615	1248	219	2367	219
nating32 MP032	7980	1549	96	1441	96
nating32 MP033	6646	1467	164	2010	164
ori32 MP027	6264	1029	211	2346	211
ori32 MP031	5423	455	78	1382	78
ori32 MP032	5420	274	47	923	47
ori32 MP033	5277	1243	298	1588	298
Total	43625	7265	1113	12057	1113

**Table 2.** Monkey site counts used for inter-cortical prediction and analyses. Dates 090817,100817,250717 correspond to neuronal activity in response to checkerboard presentations, gray screen presentations, and lights off condition. Date 260617 corresponds to small thin moving bars presentation. Date 280617 corresponds to large thick moving bars presentation. Fourth column: In the directionality prediction experiments, the area containing more sites (V1) was further subsampled to match the number of V4 sites.

Date	V1			V4	
	Total	visually responsive	Subsampled (directionality)	Total	visually responsive
090817	627	553	74	96	74
100817	688	589	81	112	81
250717	645	537	71	86	71
260617	645	593	82	86	82
280617	645	518	68	86	68
Total	3250	2829	376	469	376

504

505

## 506 Acknowledgments

507 The authors would like to thank Elisa Pavarino, Leonardo Polina, Sara Djambazovksa, Carlos Ponce,  
508 Jan Drugowitsch, and Wei-Chung Allen Lee for providing comments on the manuscript.

## 509 References

- 510 **Andermann ML**, Kerlin AM, Roumis DK, Glickfeld LL, Reid RC. Functional Specialization of Mouse Higher Visual  
511 Cortical Areas. *Neuron*. 2011 Dec; 72(6):1025–1039. [https://www.cell.com/neuron/abstract/S0896-6273\(11\)](https://www.cell.com/neuron/abstract/S0896-6273(11)01012-9)  
512 [01012-9](https://doi.org/10.1016/j.neuron.2011.11.013), doi: 10.1016/j.neuron.2011.11.013, publisher: Elsevier.
- 513 **Avitan L**, Stringer C. Not so spontaneous: Multi-dimensional representations of behaviors and context in  
514 sensory areas. *Neuron*. 2022 Oct; 110(19):3064–3075. [https://www.sciencedirect.com/science/article/pii/](https://www.sciencedirect.com/science/article/pii/S0896627322005888)  
515 [S0896627322005888](https://www.sciencedirect.com/science/article/pii/S0896627322005888), doi: 10.1016/j.neuron.2022.06.019.
- 516 **Chacron MJ**, Longtin A, Maler L. The effects of spontaneous activity, background noise, and the stimulus  
517 ensemble on information transfer in neurons. *Network (Bristol, England)*. 2003 Nov; 14(4):803–824.
- 518 **Chen X**, Morales-Gregorio A, Sprenger J, Kleinjohann A, Sridhar S, van Albada SJ, Grün S, Roelfsema PR. 1024-  
519 channel electrophysiological recordings in macaque V1 and V4 during resting state. *Scientific Data*. 2022 Mar;  
520 9(1):77. <https://www.nature.com/articles/s41597-022-01180-1>, doi: 10.1038/s41597-022-01180-1, number: 1  
521 Publisher: Nature Publishing Group.
- 522 **Connor CE**, Brincat SL, Pasupathy A. Transformation of shape information in the ventral pathway. *Current*  
523 *Opinion in Neurobiology*. 2007 Apr; 17(2):140–147. doi: 10.1016/j.conb.2007.03.002.
- 524 **Consortium M**, Bae JA, Baptiste M, Bodor AL, Brittain D, Buchanan J, Bumbarger DJ, Castro MA, Celii B, Cobos E,  
525 Collman F, Costa NMd, Dorkenwald S, Elabbady L, Fahey PG, Fliss T, Froudarakis E, Gager J, Gamlin C, Halageri  
526 A, et al. Functional connectomics spanning multiple areas of mouse visual cortex. *bioRxiv*; 2021.
- 527 **Dadarlat MC**, Stryker MP. Locomotion Enhances Neural Encoding of Visual Stimuli in Mouse V1. *The Jour-*  
528 *nal of Neuroscience: The Official Journal of the Society for Neuroscience*. 2017 Apr; 37(14):3764–3775. doi:  
529 [10.1523/JNEUROSCI.2728-16.2017](https://doi.org/10.1523/JNEUROSCI.2728-16.2017).
- 530 **Douglas RJ**, Martin KAC. Neuronal circuits of the neocortex. *Annual Review of Neuroscience*. 2004; 27:419–451.  
531 doi: 10.1146/annurev.neuro.27.070203.144152.
- 532 **Felleman DJ**, Van Essen DC. Distributed hierarchical processing in the primate cerebral cortex. *Cerebral Cortex*  
533 (New York, NY: 1991). 1991; 1(1):1–47. doi: 10.1093/cercor/1.1.1-a.
- 534 **Gazzaley A**, Rissman J, Cooney J, Rutman A, Seibert T, Clapp W, D'Esposito M. Functional Interactions be-  
535 tween Prefrontal and Visual Association Cortex Contribute to Top-Down Modulation of Visual Processing.  
536 *Cerebral Cortex*. 2007 Sep; 17(suppl\_1):i125–i135. <https://doi.org/10.1093/cercor/bhm113>, doi: 10.1093/cer-  
537 [cor/bhm113](https://doi.org/10.1093/cercor/bhm113).
- 538 **Gilbert CD**, Li W. Top-down influences on visual processing. *Nature Reviews Neuroscience*. 2013 May;  
539 14(5):350–363. <https://www.nature.com/articles/nrn3476>, doi: 10.1038/nrn3476, number: 5 Publisher: Nature  
540 Publishing Group.
- 541 **Gokcen E**, Jasper AI, Semedo JD, Zandvakili A, Kohn A, Machens CK, Yu BM. Disentangling the flow of signals  
542 between populations of neurons. *Nature Computational Science*. 2022 Aug; 2(8):512–525. [https://www.](https://www.nature.com/articles/s43588-022-00282-5)  
543 [nature.com/articles/s43588-022-00282-5](https://www.nature.com/articles/s43588-022-00282-5), doi: 10.1038/s43588-022-00282-5, number: 8 Publisher: Nature  
544 Publishing Group.
- 545 **Hohaia W**, Saurels BW, Johnston A, Yarrow K, Arnold DH. Occipital alpha-band brain waves when the eyes are  
546 closed are shaped by ongoing visual processes. *Scientific Reports*. 2022 Jan; 12:1194. [https://www.ncbi.nlm.](https://www.ncbi.nlm.nih.gov/pmc/articles/PMC8786963/)  
547 [nih.gov/pmc/articles/PMC8786963/](https://www.ncbi.nlm.nih.gov/pmc/articles/PMC8786963/), doi: 10.1038/s41598-022-05289-6.
- 548 **Hsu A**, Borst A, Theunissen FE. Quantifying variability in neural responses and its application for the val-  
549 idation of model predictions. *Network: Computation in Neural Systems*. 2004 Jan; 15(2):91–109. [https://doi.org/10.1088/0954-898X\\_15\\_2\\_002](https://doi.org/10.1088/0954-898X_15_2_002), doi: 10.1088/0954-898X\_15\_2\_002, publisher: Taylor & Francis  
550 [\\_eprint: https://doi.org/10.1088/0954-898X\\_15\\_2\\_002](https://doi.org/10.1088/0954-898X_15_2_002).
- 551
- 552 **Hubel DH**, Wiesel TN. Receptive fields, binocular interaction and functional architecture in the  
553 cat's visual cortex. *The Journal of Physiology*. 1962; 160(1):106–154. [https://onlinelibrary.](https://onlinelibrary.wiley.com/doi/abs/10.1113/jphysiol.1962.sp006837)  
554 [wiley.com/doi/abs/10.1113/jphysiol.1962.sp006837](https://onlinelibrary.wiley.com/doi/abs/10.1113/jphysiol.1962.sp006837), doi: 10.1113/jphysiol.1962.sp006837, [\\_eprint:](https://onlinelibrary.wiley.com/doi/pdf/10.1113/jphysiol.1962.sp006837)  
555 <https://onlinelibrary.wiley.com/doi/pdf/10.1113/jphysiol.1962.sp006837>.

- 556 **Ibrahim LA**, Schuman B, Bandler R, Rudy B, Fishell G. Mining the jewels of the cortex's crowning mys-  
557 tery. *Current Opinion in Neurobiology*. 2020 Aug; 63:154–161. [https://linkinghub.elsevier.com/retrieve/pii/](https://linkinghub.elsevier.com/retrieve/pii/S0959438820300842)  
558 [S0959438820300842](https://linkinghub.elsevier.com/retrieve/pii/S0959438820300842), doi: 10.1016/j.conb.2020.04.005.
- 559 **Jiang X**, Shen S, Cadwell CR, Berens P, Sinz F, Ecker AS, Patel S, Tolias AS. Principles of connectivity among  
560 morphologically defined cell types in adult neocortex. *Science*. 2015 Nov; 350(6264):aac9462. [https://www.](https://www.science.org/doi/10.1126/science.aac9462)  
561 [science.org/doi/10.1126/science.aac9462](https://www.science.org/doi/10.1126/science.aac9462), doi: 10.1126/science.aac9462, publisher: American Association for  
562 the Advancement of Science.
- 563 **Kreiman G**. *Biological and Computer Vision*. Cambridge: Cambridge University Press; 2021. [https://](https://www.cambridge.org/core/books/biological-and-computer-vision/BB7E68A69AFE7A322F68F3C4A297F3CF)  
564 [www.cambridge.org/core/books/biological-and-computer-vision/BB7E68A69AFE7A322F68F3C4A297F3CF](https://www.cambridge.org/core/books/biological-and-computer-vision/BB7E68A69AFE7A322F68F3C4A297F3CF), doi:  
565 10.1017/9781108649995.
- 566 **Lee WCA**, Bonin V, Reed M, Graham BJ, Hood G, Glatfelter K, Reid RC. Anatomy and function of an excita-  
567 tory network in the visual cortex. *Nature*. 2016 Apr; 532(7599):370–374. [https://www.nature.com/articles/](https://www.nature.com/articles/nature17192)  
568 [nature17192](https://www.nature.com/articles/nature17192), doi: 10.1038/nature17192, number: 7599 Publisher: Nature Publishing Group.
- 569 **Markov NT**, Ercsey-Ravasz MM, Ribeiro Gomes AR, Lamy C, Magrou L, Vezoli J, Misery P, Falchier A, Quilodran  
570 R, Gariel MA, Sallet J, Gamanut R, Huissoud C, Clavagnier S, Giroud P, Sappey-Marinier D, Barone P, Dehay C,  
571 Toroczkai Z, Knoblauch K, et al. A weighted and directed interareal connectivity matrix for macaque cerebral  
572 cortex. *Cerebral Cortex (New York, NY: 1991)*. 2014 Jan; 24(1):17–36. doi: 10.1093/cercor/bhs270.
- 573 **Morales-Gregorio A**, Kurth AC, Ito J, Kleinjohann A, Barthélemy FV, Brochier T, Grün S, van Albada SJ.  
574 Neural manifolds in V1 change with top-down signals from V4 targeting the foveal region. *Cell Re-*  
575 *ports*. 2024 Jul; 43(7):114371. <https://www.sciencedirect.com/science/article/pii/S2211124724006995>, doi:  
576 [10.1016/j.celrep.2024.114371](https://www.sciencedirect.com/science/article/pii/S2211124724006995).
- 577 **Niell CM**, Stryker MP. Highly Selective Receptive Fields in Mouse Visual Cortex. *The Journal of Neuroscience*.  
578 2008 Jul; 28(30):7520. <https://pmc.ncbi.nlm.nih.gov/articles/PMC3040721/>, doi: 10.1523/JNEUROSCI.0623-  
579 [08.2008](https://pmc.ncbi.nlm.nih.gov/articles/PMC3040721/).
- 580 **Niell CM**, Stryker MP. Modulation of visual responses by behavioral state in mouse visual cor-  
581 tex. *Neuron*. 2010 Feb; 65(4):472–479. <https://www.ncbi.nlm.nih.gov/pmc/articles/PMC3184003/>, doi:  
582 [10.1016/j.neuron.2010.01.033](https://www.ncbi.nlm.nih.gov/pmc/articles/PMC3184003/).
- 583 **Okazaki Y**, Abrahamyan A, Stevens CJ, Ioannides AA. The timing of face selectivity and attentional modulation  
584 in visual processing. *Neuroscience*. 2008 Apr; 152(4):1130–1144. [https://www.sciencedirect.com/science/](https://www.sciencedirect.com/science/article/pii/S0306452208001541)  
585 [article/pii/S0306452208001541](https://www.sciencedirect.com/science/article/pii/S0306452208001541), doi: 10.1016/j.neuroscience.2008.01.056.
- 586 **Papadopouli M**, Smyrnakis I, Koniotakis E, Savaglio MA, Brozi C, Psilou E, Palagina G, Smirnakis SM. Brain  
587 orchestra under spontaneous conditions: Identifying communication modules from the functional archi-  
588 tecture of area V1. *bioRxiv*. 2024 Mar; <https://www.biorxiv.org/content/10.1101/2024.02.29.582364v1>, doi:  
589 [10.1101/2024.02.29.582364](https://www.biorxiv.org/content/10.1101/2024.02.29.582364v1), pages: 2024.02.29.582364 Section: New Results.
- 590 **Park J**, Papoutsis A, Ash RT, Marin MA, Poirazi P, Smirnakis SM. Contribution of apical and basal dendrites to  
591 orientation encoding in mouse V1 L2/3 pyramidal neurons. *Nature Communications*. 2019 Nov; 10(1):5372.  
592 <https://www.nature.com/articles/s41467-019-13029-0>, doi: 10.1038/s41467-019-13029-0, publisher: Nature  
593 Publishing Group.
- 594 **Pasupathy A**, Popovkina DV, Kim T. Visual Functions of Primate Area V4. *Annual Review of Vision Science*. 2020;  
595 6(1):363–385. <https://doi.org/10.1146/annurev-vision-030320-041306>, doi: 10.1146/annurev-vision-030320-  
596 [041306](https://doi.org/10.1146/annurev-vision-030320-041306), eprint: <https://doi.org/10.1146/annurev-vision-030320-041306>.
- 597 **Petousakis KE**, Park J, Papoutsis A, Smirnakis S, Poirazi P. Modeling apical and basal tree contribution to ori-  
598 entation selectivity in a mouse primary visual cortex layer 2/3 pyramidal cell. *eLife*. 2023 Dec; 12:e91627.  
599 <https://elifesciences.org/articles/91627>, doi: 10.7554/eLife.91627.
- 600 **Polack PO**, Friedman J, Golshani P. Cellular mechanisms of brain state-dependent gain modulation in visual  
601 cortex. *Nature Neuroscience*. 2013 Sep; 16(9):1331–1339. doi: 10.1038/nn.3464.
- 602 **Reynolds JH**, Chelazzi L. Attentional modulation of visual processing. *Annual Review of Neuroscience*. 2004;  
603 27:611–647. doi: 10.1146/annurev.neuro.26.041002.131039.
- 604 **Ringach DL**. Spontaneous and driven cortical activity: implications for computation. *Current Opinion in*  
605 *Neurobiology*. 2009 Aug; 19(4):439–444. <https://www.ncbi.nlm.nih.gov/pmc/articles/PMC3319344/>, doi:  
606 [10.1016/j.conb.2009.07.005](https://www.ncbi.nlm.nih.gov/pmc/articles/PMC3319344/).

- 607 **Schmolesky MT**, Wang Y, Hanes DP, Thompson KG, Leutgeb S, Schall JD, Leventhal AG. Signal Timing Across the  
608 Macaque Visual System. *Journal of Neurophysiology*. 1998 Jun; 79(6):3272–3278. <https://journals.physiology.org/doi/full/10.1152/jn.1998.79.6.3272>, doi: 10.1152/jn.1998.79.6.3272, publisher: American Physiological  
609 Society.
- 611 **Schuman B**, Dellal S, Prönnke A, Machold R, Rudy B. Neocortical Layer 1: An Elegant Solution to Top-Down and  
612 Bottom-Up Integration. *Annual Review of Neuroscience*. 2021 Jul; 44(1):221–252. <https://www.annualreviews.org/doi/10.1146/annurev-neuro-100520-012117>, doi: 10.1146/annurev-neuro-100520-012117.  
613
- 614 **Semedo JD**, Jasper AI, Zandvakili A, Krishna A, Aschner A, Machens CK, Kohn A, Yu BM. Feedforward and feed-  
615 back interactions between visual cortical areas use different population activity patterns. *Nature Communi-*  
616 *cations*. 2022 Mar; 13(1):1099. <https://www.nature.com/articles/s41467-022-28552-w>, doi: 10.1038/s41467-  
617 022-28552-w, number: 1 Publisher: Nature Publishing Group.
- 618 **Semedo JD**, Zandvakili A, Machens CK, Yu BM, Kohn A. Cortical Areas Interact through a Communication Sub-  
619 space. *Neuron*. 2019 Apr; 102(1):249–259.e4. <https://linkinghub.elsevier.com/retrieve/pii/S0896627319300534>,  
620 doi: 10.1016/j.neuron.2019.01.026.
- 621 **Serre T**, Oliva A, Poggio T. A feedforward architecture accounts for rapid categorization. *Proceedings of*  
622 *the National Academy of Sciences*. 2007 Apr; 104(15):6424–6429. <https://www.pnas.org/doi/10.1073/pnas.0700622104>, doi: 10.1073/pnas.0700622104, publisher: Proceedings of the National Academy of Sciences.  
623
- 624 **Serre T**, Wolf L, Bileschi S, Riesenhuber M, Poggio T. Robust Object Recognition with Cortex-Like Mechanisms.  
625 *IEEE Transactions on Pattern Analysis and Machine Intelligence*. 2007 Mar; 29(3):411–426. <https://ieeexplore.ieee.org/document/4069258>, doi: 10.1109/TPAMI.2007.56, conference Name: IEEE Transactions on Pattern  
626 Analysis and Machine Intelligence.  
627
- 628 **Shen S**, Jiang X, Scala F, Fu J, Fahey P, Kobak D, Tan Z, Reimer J, Sinz F, Tolias AS. Distinct organization of two  
629 cortico-cortical feedback pathways. *bioRxiv*; 2020.
- 630 **Stringer C**, Michaelos M, Tsyboulski D, Lindo SE, Pachitariu M. High-precision coding in visual cortex. *Cell*.  
631 2021 May; 184(10):2767–2778.e15. <https://www.sciencedirect.com/science/article/pii/S0092867421003731>, doi:  
632 10.1016/j.cell.2021.03.042.
- 633 **Stringer C**, Pachitariu M, Steinmetz N, Carandini M, Harris KD. High-dimensional geometry of population re-  
634 sponses in visual cortex. *Nature*. 2019 Jun; 571(7765):361–365. <https://www.ncbi.nlm.nih.gov/pmc/articles/PMC6642054/>, doi: 10.1038/s41586-019-1346-5.  
635
- 636 **Stringer C**, Pachitariu M, Steinmetz N, Reddy CB, Carandini M, Harris KD. Spontaneous behaviors drive mul-  
637 tidimensional, brainwide activity. *Science*. 2019 Apr; 364(6437):eaav7893. <https://www.science.org/doi/10.1126/science.aav7893>, doi: 10.1126/science.aav7893, publisher: American Association for the Advancement  
638 of Science.  
639
- 640 **Talluri BC**, Kang I, Lazere A, Quinn KR, Kaliss N, Yates JL, Butts DA, Nienborg H. Activity in primate visual cortex  
641 is minimally driven by spontaneous movements. *Nature Neuroscience*. 2023 Nov; 26(11):1953–1959. <https://www.nature.com/articles/s41593-023-01459-5>, doi: 10.1038/s41593-023-01459-5, number: 11 Publisher:  
642 Nature Publishing Group.  
643
- 644 **Tang Y**, Gervais C, Moffitt R, Nareddula S, Zimmermann M, Nadew YY, Quinn CJ, Saldarriaga V, Edens P,  
645 Chubykin AA. Visual experience induces 4–8 Hz synchrony between V1 and higher-order visual areas. *Cell*  
646 *Reports*. 2023 Dec; 42(12):113482. <https://www.sciencedirect.com/science/article/pii/S2211124723014948>, doi:  
647 10.1016/j.celrep.2023.113482.
- 648 **Wang Q**, Burkhalter A. Area map of mouse visual cortex. *Journal of Comparative Neurology*. 2007;  
649 502(3):339–357. <https://onlinelibrary.wiley.com/doi/abs/10.1002/cne.21286>, doi: 10.1002/cne.21286, eprint:  
650 <https://onlinelibrary.wiley.com/doi/pdf/10.1002/cne.21286>.
- 651 **Wosniack ME**, Kirchner JH, Chao LY, Zabouri N, Lohmann C, Gjorgjieva J. Adaptation of spontaneous activ-  
652 ity in the developing visual cortex. *eLife*. 2021 Mar; 10:e61619. <https://doi.org/10.7554/eLife.61619>, doi:  
653 10.7554/eLife.61619, publisher: eLife Sciences Publications, Ltd.
- 654 **Yamins DLK**, Hong H, Cadieu CF, Solomon EA, Seibert D, DiCarlo JJ. Performance-optimized hierarchical models  
655 predict neural responses in higher visual cortex. *Proceedings of the National Academy of Sciences*. 2014  
656 Jun; 111(23):8619–8624. <http://www.pnas.org/doi/10.1073/pnas.1403112111>, doi: 10.1073/pnas.1403112111,  
657 publisher: Proceedings of the National Academy of Sciences.

## Supplemental Material

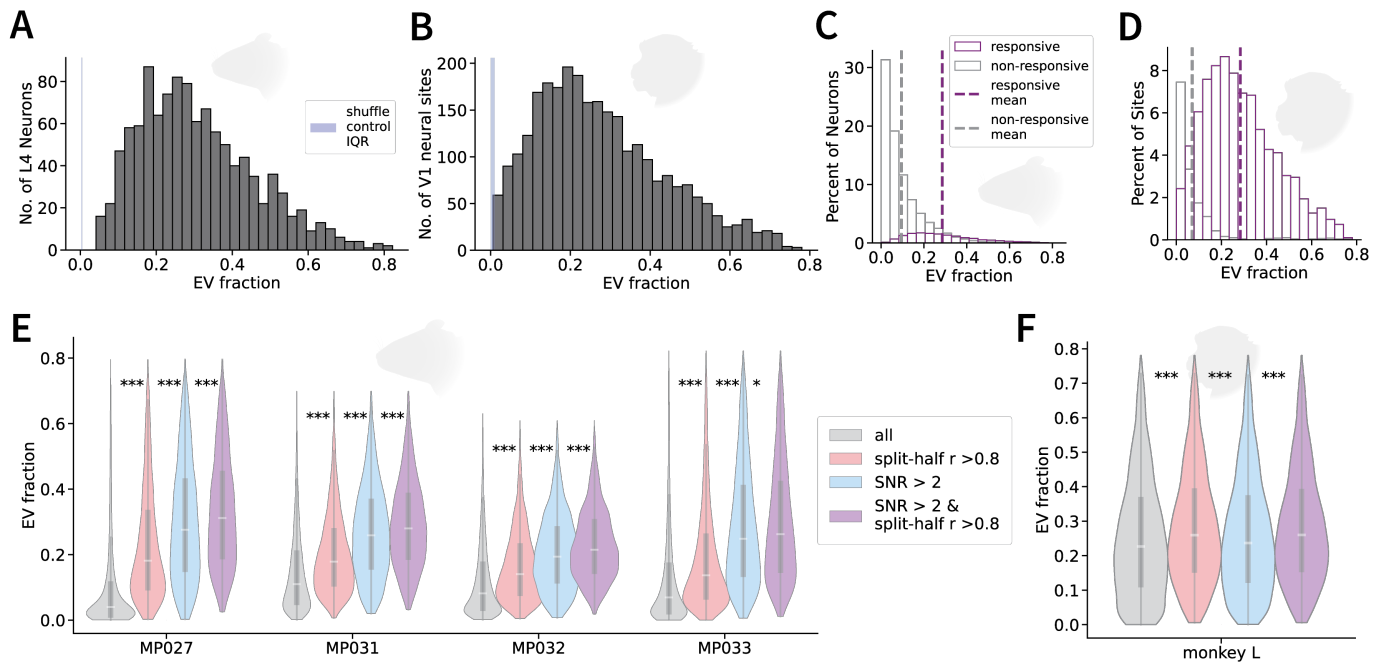


**Figure Supplement 1. EV fraction in mouse L4 neurons and macaque V1 neuronal sites and comparison between visual and non-visual neurons/sites.** **A.** Distribution of EV fraction in L2/3→L4 regressions in cells deemed visually responsive in 4 mice and 7 recording days. **B.** Same as A, but for macaque V4→V1 neuronal site regressions. **C** Distribution of visually (purple) and non-visually (gray) responsive neurons in mouse L2/3 and L4. In mouse, we used a conservative criterion to select neurons to be visually responsive, based on an average signal to noise ratio of over 2 and a split-half correlation value of at least 0.8 (more details in Methods). **D.** Same as C but for V1 and V4 sites in macaque. **E.** Differences in EV fractions using filtering methods to determine visually responsive neurons in mouse L2/3 and L4 across the 4 mice. Both a SNR of over 2 along with a split-half correlation value of over 0.8 was used to determine a neuron to be visually responsive. **F.** Same as E, but for the one macaque V1 and V4 sites.

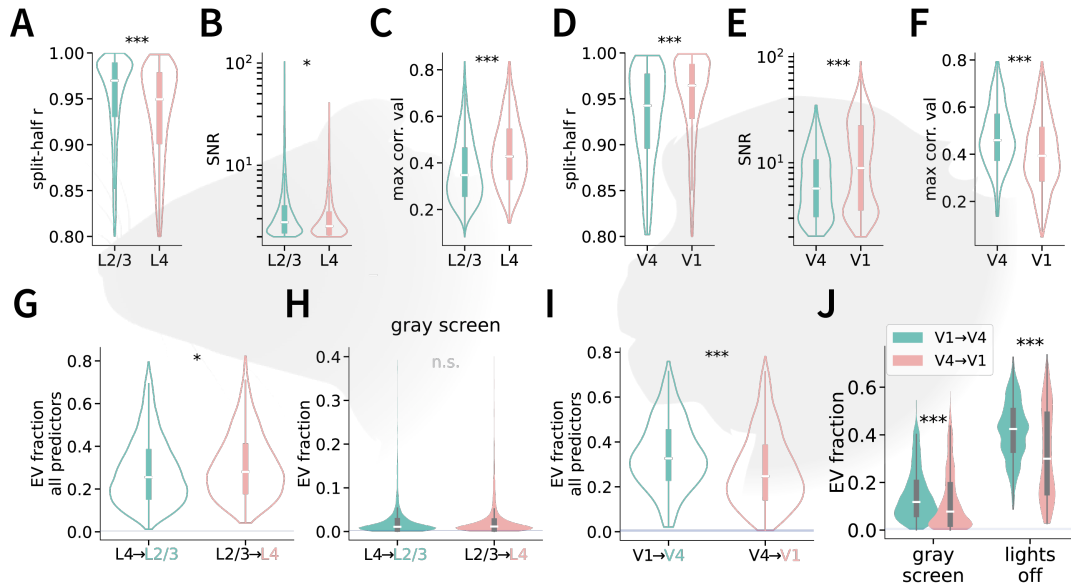


**Figure Supplement 2. Neuronal property differences between areas in mouse and monkey.** Differences in self-consistency (A), SNR (B), and max correlation value (C) between entire visually responsive neuronal populations in mouse L2/3 and L4 (independent permutation test, here and throughout figure). D-F Same as A-C but for macaque V4 and V1. G. Differences in inter-laminar predictability directions in mouse when using all predictors in their respective L2/3 and L4 layers. H. Differences in inter-laminar predictability directions in mouse during gray screen presentation neuronal activity. I. Same as G, but for macaque V1 and V4. J. Differences in inter-cortical predictability between macaque V1 and V4 neuronal activity in response to gray screen presentations and during lights off conditions.

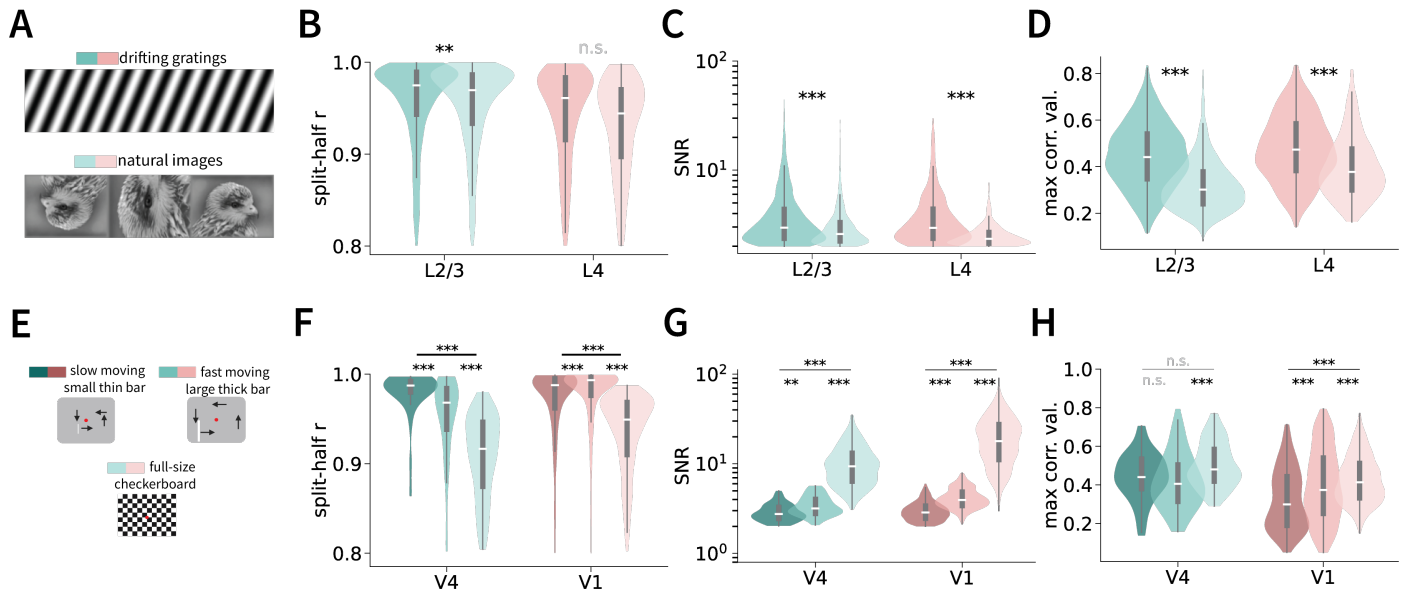


**Figure Supplement 3. neuronal activity properties for different stimulus types.** **A.** Sample stimuli for mouse drifting grating and static natural images. **B-D.** Split-half correlation (**B**), SNR (**C**), and maximum correlation values (**D**) for each mouse layer and stimulus type (see color scheme in part **A**). **E.** Sample stimuli for monkeys: full-size checkerboard, slow and fast moving bars. **F-H.** Same as **B-D** for macaque V1 and V4 (see color map for each stimulus condition in **E**).

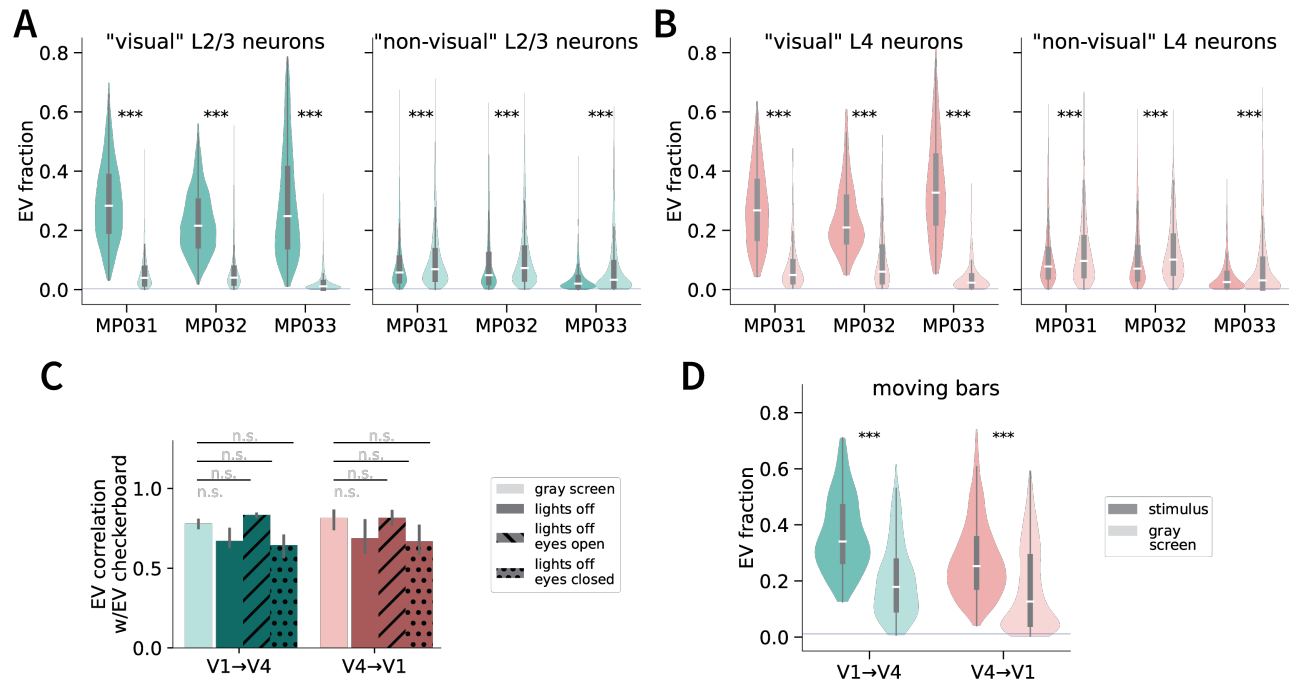


**Figure Supplement 4. Comparing stimulus presentation vs. gray screen activity predictions in mouse and macaque. A.** Differences in inter-laminar predictability between stimulus presentation and gray screen presentation neuronal activity in L2/3 across the three different mice (MP027 did not undergo gray screen presentation recordings). Left: visually responsive L2/3 neurons. Right: non-visually responsive L2/3 neurons. **B.** Same as **A**, but for mouse L4. **C.** Correlation coefficient values between checkerboard presentation and gray screen and lights off conditions in macaque inter-cortical predictability. **D.** Differences in inter-cortical predictability between moving bar presentation and gray screen activity in macaque V1 and V4 (paired permutation test).



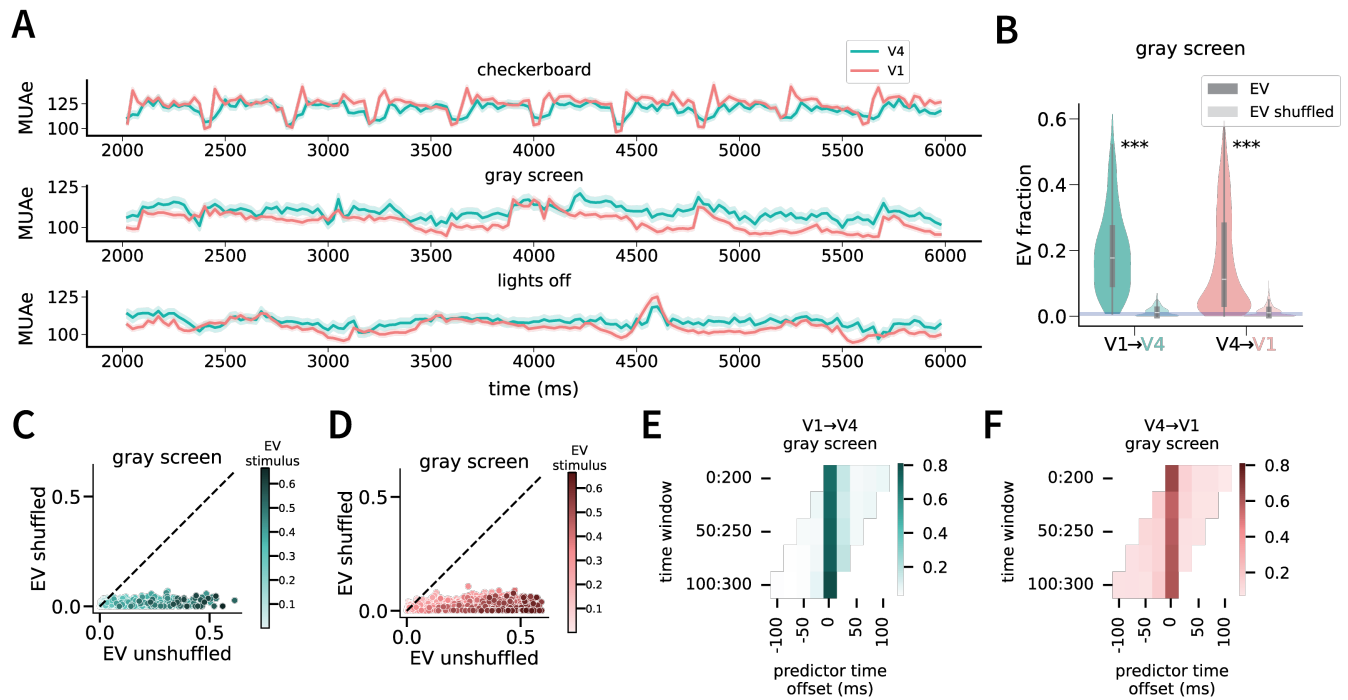


**Figure Supplement 6. Predictability across time using gray screen neuronal activity.** **A.** Sample averaged raw MUAe activity in macaque V1 and V4 across the three different conditions. **B.** Differences in EV fraction between unshuffled and shuffled trial-repeat activity during gray screen presentations (paired permutation test). Visualization of relationship between unshuffled and shuffled EV fraction in V4 (**C**) and V1 (**D**) during gray screen presentations. **E.** Percentage of neurons with max performance across predictor time offsets in V1→V4 (**E**) and V4→V1 (**F**) directions during gray screen presentations.